

# Complex-Weight Sparse Linear Array Synthesis by Bayesian Compressive Sampling

Giacomo Oliveri, *Member, IEEE*, Matteo Carlin, and Andrea Massa, *Member, IEEE*

**Abstract**—An innovative method for the synthesis of maximally sparse linear arrays matching arbitrary reference patterns is proposed. In the framework of sparseness constrained optimization, the approach exploits the multi-task (*MT*) Bayesian compressive sensing (*BCS*) theory to enable the design of complex non-Hermitian layouts with arbitrary radiation and geometrical constraints. By casting the pattern matching problem into a probabilistic formulation, a Relevance-Vector-Machine (*RVM*) technique is used as solution tool. The numerical assessment points out the advances of the proposed implementation over the extension to complex patterns of [18] and it gives some indications about the reliability, flexibility, and numerical efficiency of the *MT*–*BCS* approach also in comparison with state-of-the-art sparse-arrays synthesis methods.

**Index Terms**—Array synthesis, Bayesian compressive sampling, complex-weight pattern, linear arrays, shaped-beam pattern, sparse arrays.

## I. INTRODUCTION AND MOTIVATION

**R**ADAR tracking, biomedical imaging, satellite and ground communications, and remote sensing applications require antenna patterns with suitable sidelobes, null positions, mainlobe size and shape, and directivity [1]. To synthesize shaped-beam arrays, several approaches especially concerned with uniformly-spaced arrangements [1]–[5] have been proposed over the last sixty years. Although successful in some applications, uniform arrays have the limitation to be expensive and heavy when wide apertures are at hand [1] since a huge amount of radiating elements spaced by  $\lambda/2$  are needed to avoid grating lobes [6]. Therefore, non-uniform arrangements have been naturally proposed [6]–[11] because of their advantages over their regularly-spaced counterparts (e.g., resolution [12], sidelobe level control/reduction [13], and efficiency in dealing with physically constrained geometries [14]). State-of-the-art solutions usually consider *thinned* regular arrangements to yield a minimum peak sidelobe level (*PSL*) [1], [10], [15], [16] or *sparse* layouts with the minimum number of radiating elements given a desired pattern [11], [17], [18]. Whether several techniques as random thinning [19], [20], dynamic programming [21], genetic algorithms

[22]–[24], analytical approaches [10], [15], [25], and hybrid methodologies [26]–[29] have been investigated for array thinning, few methods have been so far proposed for synthesizing sparse arrangements [11], [17], [18], [30], [31]. As for these latter, steepest descent [32], iterative least squares [33], simplex search [6], and linear programming [34] methodologies have been firstly developed because of their efficiency. Improved performances have been successively reached by using recursive inversion techniques [35], [36], stochastic optimizers [17], generalized Gaussian quadrature approaches [37], and the matrix pencil method (*MPM*) [11], [30], [31]. More recently, a new approach based on the Bayesian compressive sensing (*BCS*) [38] has been proposed for the design of sparse layouts matching user-defined reference patterns [18]. The so-called “*BCS* technique” has been formulated starting from a probabilistic description of the array synthesis [18] then solved by exploiting an efficient fast relevance vector machine (*RVM*) [38]. Thanks to its efficiency, the *BCS* syntheses usually positively compares with state-of-the-art methodologies in terms of flexibility, synthesis time, and number of array elements, while guaranteeing an excellent pattern matching [18]. However, such a formulation deals with symmetric purely-real arrangements and its extension to complex syntheses is not efficient because of the real-valued nature of the *BCS* solver itself [38]. Consequently, this work is aimed at proposing, still in the framework of the probabilistic sparseness constrained optimization, an innovative, flexible, and numerically efficient complements to state-of-the-art approaches for the synthesis of maximally sparse linear arrays matching a (possibly complex) reference pattern. Following the guidelines in [18] to recast the complex-valued synthesis in probabilistic terms and suitably reformulating the original pattern-matching problem in an equivalent “fictitious” one (11), a multi-task Bayesian Compressive Sensing (*MT*–*BCS*) methodology [39] is applied. Unlike the *BCS* extension where the real and the imaginary components of the sparse excitation vector are dealt with as independent, a “shared-prior” [39] is exploited to enforce the synthesis of complex excitations rather than purely real and/or imaginary weights.

The paper is organized as follows. The sparse synthesis of complex-weight linear arrays is mathematically formulated in a probabilistic fashion and the *MT*–*BCS* method is presented (Section II). Representative results of an extensive set of numerical simulations are presented to validate the proposed approach, to assess its advances over the *BCS* extension to complex patterns, and to compare its performances with those of state-of-the-art techniques (Section III). Finally, some conclusions are drawn (Section IV).

Manuscript received August 07, 2011; revised September 24, 2011; accepted November 11, 2011. Date of publication March 02, 2012; date of current version May 01, 2012.

The authors are with the ELEDIA Research Center DISI, University of Trento, Povo 38050 Trento, Italy (e-mail: giacomo.oliveri@ing.unitn.it; matteo.carlin@disi.unitn.it; andrea.massa@ing.unitn.it).

Color versions of one or more of the figures in this paper are available online at <http://ieeexplore.ieee.org>.

Digital Object Identifier 10.1109/TAP.2012.2189742

## II. MATHEMATICAL FORMULATION

### A. Array Synthesis Problem

The problem of synthesizing a (complex and non-symmetric) sparse linear array with a prescribed radiated pattern can be formulated as follows [18]

**Array Synthesis Problem**—Find the minimum  $P$  value and the corresponding sparse array descriptors  $\mathbf{v} = \{v_p; p = 1, \dots, P\}$  and  $\mathbf{l} = \{l_p; p = 1, \dots, P\}$  that satisfy the matching constraint

$$\sum_{k=1}^K \left| F_{REF}(u_k) - \sum_{p=1}^P v_p \exp(i2\pi l_p u_k) \right|^2 \leq \epsilon. \quad (1)$$

In (1),  $\epsilon$  is the “fidelity factor”,  $v_p$  and  $l_p$  are the complex ( $v_p \in \mathbb{C}$ ) weight and the position in wavelengths ( $l_p \in \mathbb{R}$ ) of the  $p$ -th array element, respectively, while  $F_{REF}(u_k) \in \mathbb{C}$  is the  $k$ -th ( $k = 1, \dots, K$ ) sample of the reference pattern at the observation angle  $u_k$  within the angular range  $[-1, 1]$ . Similarly to [6], [18], the  $P$  element positions are assumed to belong to a user-chosen set of  $N$  ( $N \gg P$ ) arbitrary candidate locations  $\mathbf{d} = \{d_n; n = 1, \dots, N\}$  to straightforwardly integrate geometrical constraints in the synthesis process [18]. Equation (1) is then recast into the following sparse matrix form [40], [18]

$$\mathbf{F}_{REF} - \Phi \mathbf{w} = \mathcal{D} \quad (2)$$

by introducing the sparse<sup>1</sup> weight vector  $\mathbf{w} = \{w_n; n = 1, \dots, N\}$

$$w_n = \begin{cases} v_p & \text{if } d_n = l_p \\ 0 & \text{otherwise,} \end{cases} \quad (3)$$

where  $\mathbf{F}_{REF} = \{F_{REF}(u_k); k = 1, \dots, K\}$ ,  $\mathcal{D} = \{\Delta_k; k = 1, \dots, K\}$  is a vector of zero-mean complex Gaussian entries with variance  $\sigma^2$  proportional to  $\epsilon$  [38], [40], [41], and

$$\Phi \triangleq \begin{bmatrix} \exp\left(\frac{i2\pi d_1 u_1}{\lambda}\right) & \cdots & \exp\left(\frac{i2\pi d_N u_1}{\lambda}\right) \\ \vdots & \ddots & \vdots \\ \exp\left(\frac{i2\pi d_1 u_K}{\lambda}\right) & \cdots & \exp\left(\frac{i2\pi d_N u_K}{\lambda}\right) \end{bmatrix} \quad (4)$$

is the “observation matrix” [38]. Thanks to this “sparse” description, the *Antenna Synthesis Problem* can be also formulated as follows

**Sparse Vector Synthesis Problem**—Find the minimum  $\ell_0$ -norm weight vector  $\mathbf{w}$  ( $\mathbf{w} \in \mathbb{C}^N$ ) that satisfies (2) where

$$\|\mathbf{w}\|_{\ell_0} \triangleq \sum_{n=1}^N |w_n|^0 = \sum_{p=1}^P |v_n|^0 = P. \quad (5)$$

Once  $\mathbf{w}$  is found, the unknowns  $\mathbf{v}$  and  $\mathbf{l}$  of the *Antenna Synthesis Problem* are computed as detailed in Fig. 1.

<sup>1</sup>It is worth remarking that  $\mathbf{w}$  turns out a *sparse* vector since  $N \gg P$ .

- Step 0.** Get input values of  $N$  and  $w_n$  ( $n = 1, \dots, N$ );
- Step 1.** Set  $p = 1, n = 1$ ;
- Step 2.** If  $w_n \neq 0$ , set  $l_p = d_n$ ,  $v_p = w_n$ , and  $p = p + 1$ ;
- Step 3.** If  $n < N$ , set  $n = n + 1$  and goto 2; else goto 4.
- Step 4.** Return output values of  $P$ ,  $\mathbf{l}_p$  and  $\mathbf{v}_p$  ( $p = 1, \dots, P$ )

Fig. 1. Computation of the complex weights  $v_p \in \mathbb{C}$  and element positions  $l_p \in \mathbb{R}$  ( $p = 1, \dots, P$ ) starting from the sparse vector  $\mathbf{w} \in \mathbb{C}^N$ .

### B. BCS Synthesis Method

The solution of the *Sparse Vector Synthesis Problem* cannot be yielded through the method described in [18], since the *BCS* approach addresses purely real-valued problems [18], [38], while (2) generally includes complex-valued vectors and matrices. To directly extend the approach in [18] to the complex formulation at hand, (2) is manipulated as follows

$$\tilde{\mathbf{F}}_{REF} - \tilde{\Phi} \tilde{\mathbf{w}} = \tilde{\mathcal{D}} \quad (6)$$

by defining  $\tilde{\mathbf{w}} = [\mathcal{R}\{\mathbf{w}\}, \mathcal{I}\{\mathbf{w}\}]$  ( $\tilde{\mathbf{w}} \in \mathbb{R}^{2N}$ ),  $\tilde{\mathbf{F}}_{REF} = [\mathcal{R}\{\mathbf{F}_{REF}\}, \mathcal{I}\{\mathbf{F}_{REF}\}]$  ( $\tilde{\mathbf{F}}_{REF} \in \mathbb{R}^{2K}$ ),  $\tilde{\mathcal{D}} = [\mathcal{R}\{\mathcal{D}\}, \mathcal{I}\{\mathcal{D}\}]$  ( $\tilde{\mathcal{D}} \in \mathbb{R}^{2K}$ ), and  $\tilde{\Phi} = [\mathcal{R}\{\Phi\} \ -\mathcal{I}\{\Phi\} \ \mathcal{I}\{\Phi\} \ \mathcal{R}\{\Phi\}]$  ( $\tilde{\Phi} \in \mathbb{R}^{2K \times 2N}$ ), where  $\mathcal{R}\{\cdot\}$  and  $\mathcal{I}\{\cdot\}$  stand for the real and the imaginary part, respectively. Accordingly, the following extended real-valued problem can be then formulated

**BCS “Deterministic” Synthesis Problem**—Find the minimum  $\ell_0$ -norm “extended” weight vector  $\tilde{\mathbf{w}}$  ( $\tilde{\mathbf{w}} \in \mathbb{R}^{2N}$ ) that satisfies (6).

and successively expressed in the *probabilistic* framework [18]

**BCS “Probabilistic” Synthesis Problem**—Find the minimum  $\ell_0$ -norm “extended” weight vector  $\tilde{\mathbf{w}}$  ( $\tilde{\mathbf{w}} \in \mathbb{R}^{2N}$ ) subject to

$$\tilde{\mathbf{w}}^{BCS} = \arg \left[ \max_{\tilde{\mathbf{w}}} \mathcal{P} \left( \tilde{\mathbf{w}} | \tilde{\mathbf{F}}_{REF} \right) \right] \quad (7)$$

whose (real-valued) solution is given by [18]

$$\tilde{\mathbf{w}}^{BCS} = \frac{1}{\tilde{\sigma}_{BCS}^2} \left( \frac{\tilde{\Phi}^T \tilde{\Phi}}{\tilde{\sigma}_{BCS}^2} + \tilde{\mathbf{a}}^{BCS} \right)^{-1} \tilde{\Phi}^T \tilde{\mathbf{F}}_{REF} \quad (8)$$

where  $\tilde{\sigma}_{BCS}^2$  is the estimated variance of  $\Delta_k$  ( $k = 1, \dots, K$ ) and  $\tilde{\mathbf{a}}^{BCS}$  ( $\tilde{\mathbf{a}}^{BCS} \in \mathbb{R}^{2N}$ ) is the hyperparameter vector, whose  $n$ -th entry,  $\tilde{a}_n^{BCS}$ , controls the strength of the sparseness prior over  $\tilde{w}_n^{BCS}$  [42]. These parameters are computed by maximizing the logarithm of the *BCS* “marginal likelihood”,  $\mathcal{L}^{BCS}(\tilde{\mathbf{a}}, \sigma^2)$  [18]

$$\begin{aligned} & \mathcal{L}^{BCS}(\tilde{\mathbf{a}}, \sigma^2) \\ &= -\frac{1}{2} \left[ (2N) \log 2\pi + \log |\tilde{C}| + \tilde{\mathbf{F}}_{REF}^T (\tilde{C})^{-1} \tilde{\mathbf{F}}_{REF} \right] \end{aligned} \quad (9)$$

where  $\tilde{C} \triangleq \sigma^2 I + \tilde{\Phi} [\tilde{A}]^{-1} \tilde{\Phi}^T$ , and  $\tilde{A} = \text{diag}(\tilde{\mathbf{a}})$ .

Finally, the  $N$  entries of the weight vector  $\mathbf{w}^{BCS}$  ( $\mathbf{w}^{BCS} \in \mathbb{C}^N$ ) are found as

$$w_n^{BCS} = \tilde{w}_n^{BCS} + i\tilde{w}_{n+N}^{BCS}, \quad n = 1, \dots, N. \quad (10)$$

Equation (8) provides a direct extension of the method in [18] to deal with complex and non-symmetric arrays. However, such a solution bears an intrinsic limitation. The real ( $\mathcal{R}\{w_n^{BCS}\} = \tilde{w}_n^{BCS}$ ,  $n = 1, \dots, N$ ) and imaginary ( $\mathcal{I}\{w_n^{BCS}\} = \tilde{w}_{n+N}^{BCS}$ ,  $n = 1, \dots, N$ ) parts of the weights are managed as independent quantities—see (6)—since each  $\tilde{w}_n^{BCS} \in \mathbb{R}$  ( $n = 1, \dots, 2N$ ) is treated as statistically independent. See (4)–(6) in [18]. This in turns leads to sparse *BCS* layouts where the array weights  $v_p$  ( $p = 1, \dots, P$ ) are often either purely real or purely imaginary, neglecting that sparse *complex* layouts frequently exhibit non-negligible real and imaginary components at the same array locations. Such a drawback generally does not enable the approach to synthesize very sparse layouts with a good reference pattern matching, as it has been confirmed by the numerical analysis whose representative results will be presented in Section III.

### C. MT – BCS Synthesis Method

To overcome the limitations of *BCS Synthesis Method* (Section II-B), the *MT – BCS* approach [39] is exploited and suitably customized for statistically modelling the relations between the real and imaginary parts of the array weights. Towards this end, (2) is firstly rewritten in terms of the *fictitious* weights vectors  $\mathbf{w}_R \triangleq \mathcal{R}\{\mathbf{w}\}$  and  $\mathbf{w}_I \triangleq \mathcal{I}\{\mathbf{w}\}$  ( $\mathbf{w}_I, \mathbf{w}_R \in \mathbb{R}^N$ )

$$\begin{cases} \hat{\mathbf{F}}_R - \hat{\Phi} \mathbf{w}_R = \hat{\mathcal{D}}_R \\ \hat{\mathbf{F}}_I - \hat{\Phi} \mathbf{w}_I = \hat{\mathcal{D}}_I \end{cases} \quad (11)$$

where  $\hat{\mathcal{D}}_R \in \mathbb{R}^{2K}$  and  $\hat{\mathcal{D}}_I \in \mathbb{R}^{2K}$  are zero-mean complex Gaussian error vectors (with variance  $\sigma^2/2$ ) such that  $\hat{\mathcal{D}}_R + \hat{\mathcal{D}}_I = \hat{\mathcal{D}}$ ,  $\hat{\Phi} \triangleq [\mathcal{R}\{\Phi\}, \mathcal{I}\{\Phi\}]$  is the *MT* observation matrix, while  $\hat{\mathbf{F}}_R = [\mathcal{R}\{\mathbf{F}_R\}, \mathcal{I}\{\mathbf{F}_R\}]$  and  $\hat{\mathbf{F}}_I = [\mathcal{R}\{\mathbf{F}_I\}, \mathcal{I}\{\mathbf{F}_I\}]$  ( $\hat{\mathbf{F}}_R, \hat{\mathbf{F}}_I \in \mathbb{R}^{2K}$ ). Moreover,  $\mathbf{F}_R \in \mathbb{C}^K$  and  $\mathbf{F}_I \in \mathbb{C}^K$  satisfy the following condition

$$\mathbf{F}_R + i\mathbf{F}_I = \mathbf{F}_{REF}. \quad (12)$$

Accordingly, the *multi-task* (real-valued) problem turns out to be

***MT – BCS “Deterministic” Synthesis Problem***—Find the minimum  $\ell_0$ -norm “fictitious” weight vectors  $\mathbf{w}_R$  and  $\mathbf{w}_I$  ( $\mathbf{w}_I, \mathbf{w}_R \in \mathbb{R}^N$ ) that satisfy (11) and as follows into the *probabilistic* framework [39]

***MT – BCS “Probabilistic” Synthesis Problem***—Find the minimum  $\ell_0$ -norm “fictitious” weight vectors  $\mathbf{w}_R$  and  $\mathbf{w}_I$  ( $\mathbf{w}_I, \mathbf{w}_R \in \mathbb{R}^N$ ) subject to

$$\begin{cases} \mathbf{w}_R^{MT-BCS} = \arg \left[ \max_{\mathbf{w}_R} \mathcal{P}(\mathbf{w}_R | \hat{\mathbf{F}}_R) \right] \\ \mathbf{w}_I^{MT-BCS} = \arg \left[ \max_{\mathbf{w}_I} \mathcal{P}(\mathbf{w}_I | \hat{\mathbf{F}}_I) \right] \end{cases} \quad (13)$$

whose (real-valued) solution are given by

$$\mathbf{w}_H^{MT-BCS} = \left( \text{diag}(\hat{\mathbf{a}}^{MT-BCS}) + \hat{\Phi}^T \hat{\Phi} \right)^{-1} \hat{\Phi}^T \hat{\mathbf{F}}_H, \quad H \in \{R, I\}, \quad (14)$$

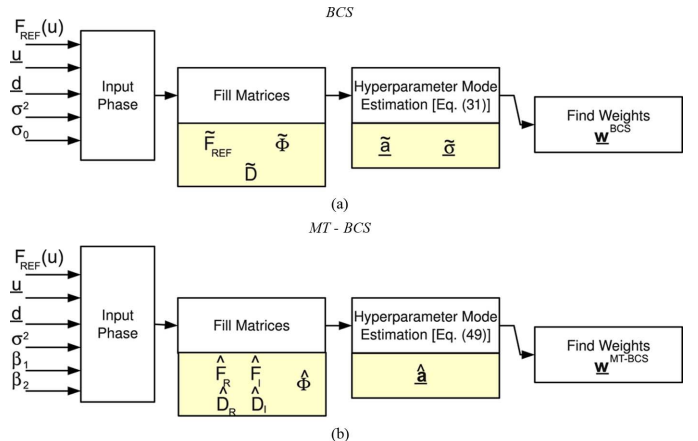


Fig. 2. Sparse Synthesis Flowchart (a) *BCS* method ( $\sigma_0$  being the initial estimate of  $\sigma$  [18]) and (b) *MT – BCS* method.

while the corresponding estimated weight vector turns out to be

$$\mathbf{w}^{MT-BCS} = \mathbf{w}_R^{MT-BCS} + i\mathbf{w}_I^{MT-BCS}. \quad (15)$$

See the Appendix.

### D. MT – BCS Algorithmic Implementations

The algorithmic implementation of the *MT – BCS* technique consists of the following steps (Fig. 2(b)):

- 1) *Input Phase*—Set the reference pattern  $F_{REF}(u)$ , the grid of admissible locations ( $d$ ), the set of pattern sampling points ( $u$ ), the target variance  $\sigma^2$  of the error term  $\mathcal{D}$ , and the user-defined scale priors  $\beta_1$  and  $\beta_2$  (19) [39];
- 2) *Matrix Definition*—Fill the entries of the vectors  $\hat{\mathbf{F}}_R$ ,  $\hat{\mathbf{F}}_I$ ,  $\hat{\Phi}$ ,  $\hat{\mathcal{D}}_R$ , and  $\hat{\mathcal{D}}_I$ ;
- 3) *Hyperparameter Posterior Modes Estimation*—Find  $\hat{\mathbf{a}}^{MT-BCS}$  by maximizing (30) [39];
- 4) *Array Weights Estimation*—Find  $\mathbf{w}^{MT-BCS}$  by (15);
- 5) *Output Phase*—Compute  $P_{MT-BCS}$ ,  $\mathbf{v}^{MT-BCS}$ , and  $\mathbf{l}^{MT-BCS}$  (Fig. 1).

By comparing the algorithmic descriptions of the *BCS* (Section III of [18] and Fig. 2(a)) and *MT – BCS* (Section II-D—Fig. 2(b)), it is observed that both approaches require  $d$ ,  $u$ , and  $\sigma^2$ , while the *MT – BCS* needs the definition of the scale priors  $\beta_1$  and  $\beta_2$  instead of the initial estimates  $\sigma_0^2$  as for the *BCS*. Thanks to these differences and unlike the *BCS* approach, the *MT – BCS*

- enables the *explicit* model and control of the relationships between the real and imaginary parts of the array weights thanks to the specification of  $\beta_1$  and  $\beta_2$  in (19);
- requires neither some *a-priori* knowledge/information on the noise (e.g.,  $\sigma_0^2$ ) nor the estimation of the noise level (i.e.,  $\tilde{\sigma}^2$ ) for determining the problem solution.

## III. NUMERICAL RESULTS

The objectives of this section are two-fold: On the one hand, it provides guidelines for applying the *MT – BCS* method to the synthesis of sparse complex layouts. On the other hand, it assesses the method’s effectiveness in both reducing the number of array elements and accurately matching reference patterns,

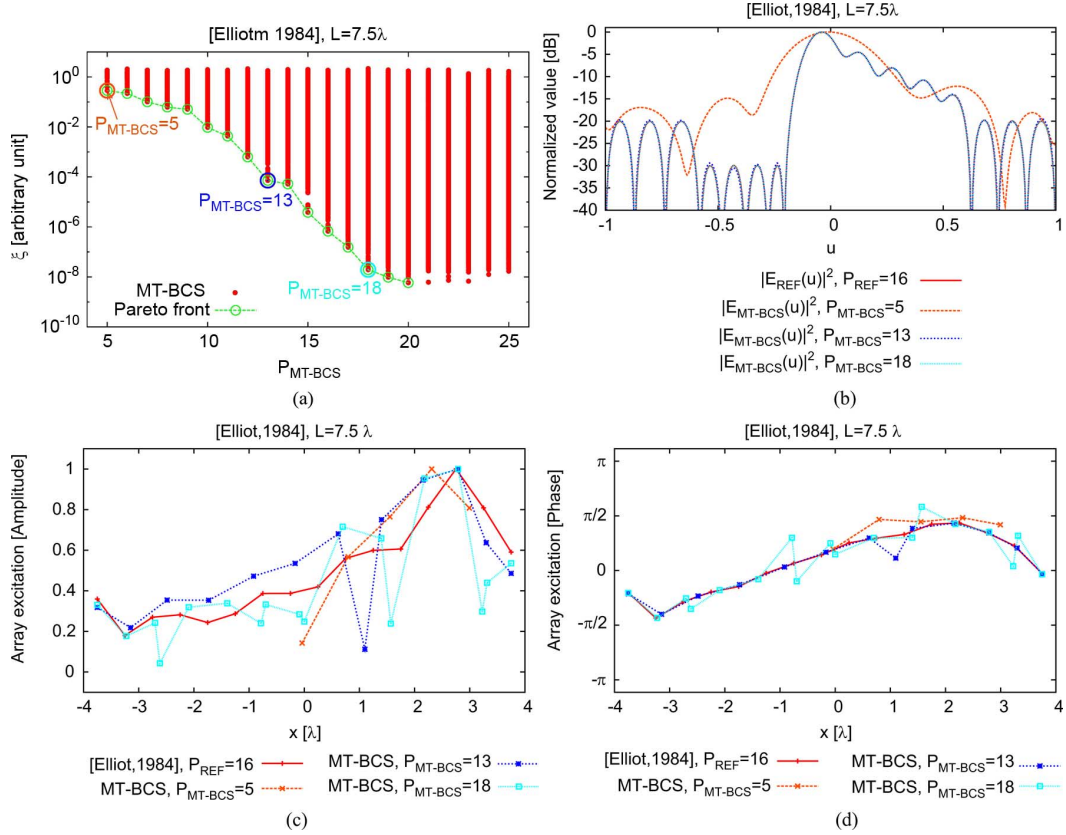


Fig. 3. *MT – BCS Sensitivity Analysis (Shaped Pattern Synthesis):  $L = 7.5\lambda$*  [2]—Plot of the representative points of a set of *MT – BCS* solutions in the  $(\xi, P_{MTBCS})$  plane (a). Power patterns (b), excitation amplitudes (c) and phases (d) of the reference and of the set of representative *MT – BCS* arrays circled in (a).

with the assessment made by comparing the *MT – BCS* results with those of other reliable, state-of-the-art (regular and sparse) array synthesis methodologies. For the assessment, the following quantities are analyzed: the normalized matching error,  $\xi$ ,

$$\xi \triangleq \frac{\int_{-1}^1 \left| F_{REF}(u) - \sum_{p=1}^P v_p \exp(i2\pi l_p u) \right|^2 du}{\int_{-1}^1 |F_{REF}(u)|^2 du},$$

the aperture length,  $L$ , ( $L \triangleq |l_P - l_1|$ ), the mean ( $\Delta L \triangleq L/P - 1$ ), and the minimum ( $\Delta L_{\min} \triangleq \min_{p=1,\dots,P-1} \{ |l_{p+1} - l_p| \}$ ) inter-element spacing.

#### A. Sensitivity Analysis

The first set of numerical experiments is concerned with the sensitivity of the *MT – BCS* synthesis on its control parameters, while the reader is referred to [18] for the calibration of the *BCS* approach. Towards this purpose, the synthesis of a non-uniform array matching a complex-weight “cosecant” pattern with  $L = 7.5\lambda$  and  $PSL = -20$  dB is assumed as reference test case (Fig. 3(b)). Such a pattern can be synthesized by a uniform layout of  $P_{UNI} = 16$  elements  $\lambda/2$ -spaced [2]. The *MT – BCS* synthesis is carried out by assuming

$$u_k = -1 + \frac{2k}{K} \quad k = 1, \dots, K$$

and setting the uniform grid of  $N$  candidate locations as follows  $d_n = L(-1/2 + n/N)$ ,  $n = 1, \dots, N$ . Fig. 3(a) shows the representative points of the synthesized *MT – BCS* sparse layouts in the  $\xi – P_{MTBCS}$  plane, along with the associated Pareto front in such a plane, when varying the control parameters within the ranges:  $N = \{25, \dots, 800\}$ ,  $K = \{10, \dots, 30\}$ ,  $\sigma^2 = \{10^{-5}, 5.0 \times 10^{-1}\}$ ,  $\beta_1 = \{10^{-2}, 10^3\}$ , and  $\beta_2 = \{10^{-2}, 10^3\}$ . These results show that the values of the pattern matching accuracy lie in the range  $\xi \in [10^{-8}, 2]$  with a number of array elements ranging from a minimum of  $P_{MTBCS} = 5$  up to a maximum of  $P_{MTBCS} = 25$  (Fig. 3(a)). By analyzing the synthesized pattern for three Pareto solutions, namely  $P_{MTBCS} = \{5, 13, 18\}$  [Fig. 3(b)], it turns out that the sparsest solution ( $P_{MTBCS} = 5$ ) yields a poor approximation of the reference pattern as also confirmed by the corresponding matching error [ $\xi = 2.86 \times 10^{-1}$ —Fig. 3(a)], while a good fitting is reached when  $P_{MTBCS} = 13$  active elements are at hand [ $\xi = 7.24 \times 10^{-5}$ —Fig. 3(a)]. A further reduction of the matching error [e.g.,  $\xi = 2.83 \times 10^{-7}$ —Fig. 3(a)] by using a larger number of elements ( $P_{MTBCS} = 18$ ) does not provide significant improvements. Therefore, analogous to the guidelines deduced in [18], an accuracy index close to or below  $\xi_{th} = 10^{-4}$  is identified as the optimal threshold for obtaining a suitable trade-off between pattern matching and reduction of the number of elements (i.e.,  $P_{MTBCS}/P_{UNI}$ ). As for the associated array structure, the optimal trade-off *MT – BCS* layout (i.e.,  $P_{MTBCS} = 13 - \xi = 7.24 \times 10^{-5}$ ) exhibits a distribution

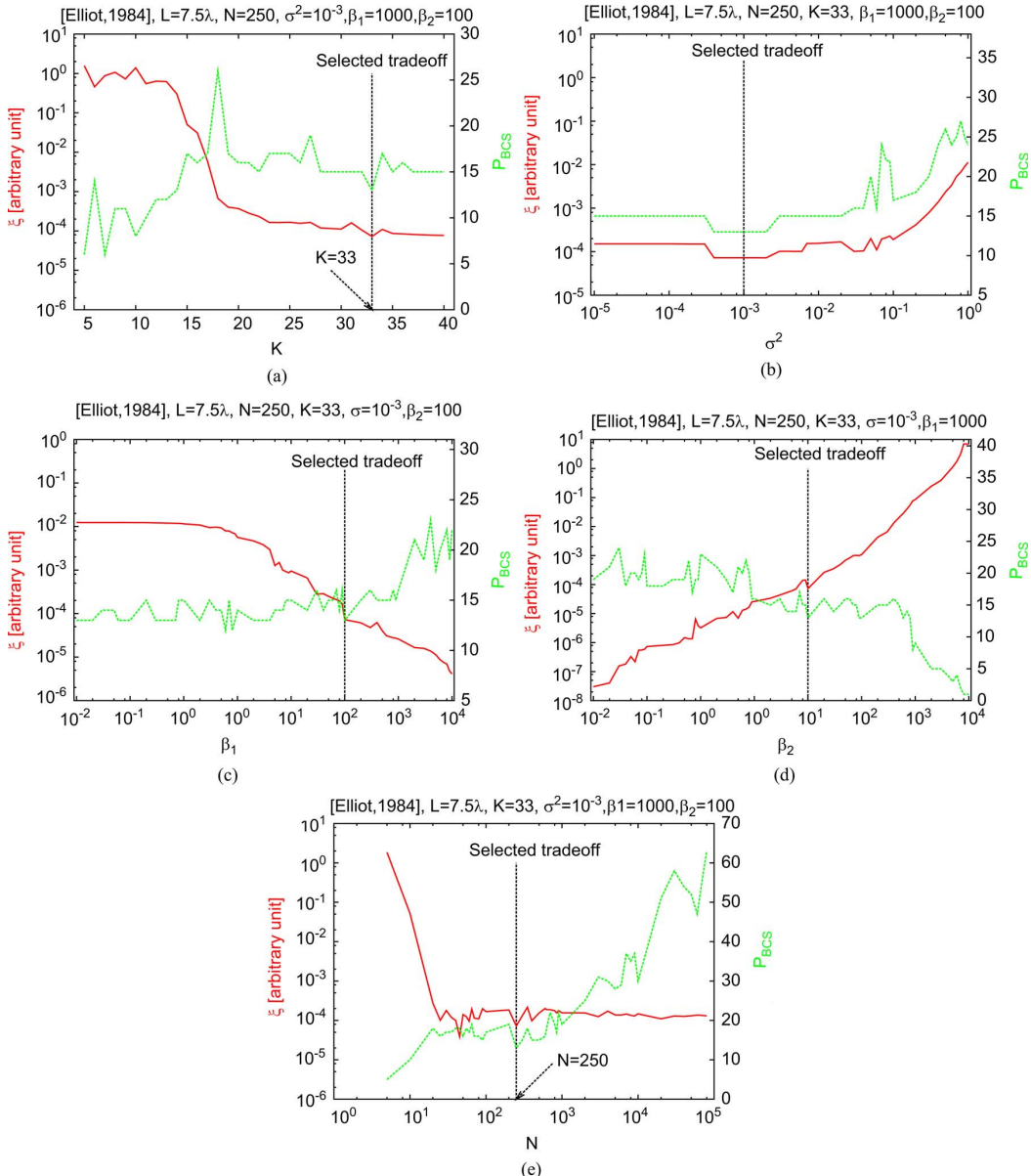


Fig. 4.  $MT - BCS$  Sensitivity Analysis (Shaped Pattern Synthesis:  $L = 7.5\lambda$  [2]—Behaviours of  $\xi$  and  $P_{MT-BCS}$  versus (a)  $K$  (b)  $\sigma^2$  (c)  $\beta_1$  (d)  $\beta_2$ , and (e)  $N$ .

of the array weights similar to that of the corresponding uniform architecture [2], although with a non-uniform, and larger, on the average, inter-element spacing [Fig. 3(c)–(d)]. This suggests that the method performs an implicit non-uniform sampling of the ideal current distribution synthesizing  $F_{REF}(u)$  [Fig. 3(c)–(d)]. On the contrary, the non-optimal trade-off solutions differ quite significantly from the uniform distribution case [e.g.,  $L_{MTBCS}/L_{UNI} \approx 0.4$  when  $P_{MTBCS} = 5$ —Fig. 3(c)].

Fig. 4 completes the sensitivity analysis carried out for calibrating the  $MT - BCS$ . Each plot gives the values of  $\xi$  and  $P_{MTBCS}$  versus a control parameter (i.e.,  $K$ ,  $\sigma^2$ ,  $\beta_1$ ,  $\beta_2$ , and  $N$ ) by setting the others to the optimal trade-off setup (i.e.,  $P_{MTBCS} = 13 - K = 33$ ,  $N = 250$ ,  $\sigma = 10^{-3}$ ,  $\beta_1 = 10^3$ ,  $\beta_2 = 10^2$ ).

By analyzing the behavior of  $\xi$  as a function of  $K$  [Fig. 4(a)], it turns out that increasing the number of samples of the reference pattern up to the Nyquist threshold ( $K_{Nyquist} = 2 \times$

$P_{UNI} - 1 = 31$  [11]) gives a non-negligible reduction of the matching error  $\xi$ , while further increments only slightly modify the matching accuracy or  $P_{MTBCS}$ . Accordingly, a sampling threshold within  $K \in [K_{Nyquist}, 1.2K_{Nyquist}]$  has been assumed in the following analyses.

Concerning the dependence of  $\xi$  and  $P_{MTBCS}$  on  $\sigma^2$ , Fig. 4(b) shows that the values of the two indexes are almost constant when  $\sigma^2 \leq 3 \times 10^{-2}$ , while they increase otherwise. Such a behavior is actually expected from the  $MT - BCS$  theory. See Section II-C and the Appendix. Indeed, larger  $\sigma^2$  values correspond to less accurate pattern approximations [see (2)] as well as less sparsely filled layouts. Consequently, good trade-offs between accuracy and sparseness are expected by choosing  $\sigma^2 \in [10^{-4}, 10^{-2}]$ .

With reference to the  $MT - BCS$  sensitivity to the scale prior  $\beta_1$ ,  $\xi$  reduces as the prior value is enlarged [Fig. 4(c)], even though such a matching improvement is obtained by in-

TABLE I  
UNCONSTRAINED SYNTHESIS—ARRAY PERFORMANCE INDEXES

Reference Pattern			BCS						MT—BCS					
$L[\lambda]$	$P_{UNI}$	Type	$\xi [\times 10^{-4}]$	$\frac{P_{BCS}}{P_{UNI}}$	$\frac{\Delta L_{min}}{\lambda/2}$	$\frac{\Delta L}{\lambda/2}$	$\frac{L_{BCS}}{L}$	$\Delta t$	$\xi [\times 10^{-4}]$	$\frac{P_{MTBCS}}{P_{UNI}}$	$\frac{\Delta L_{min}}{\lambda/2}$	$\frac{\Delta L}{\lambda/2}$	$\frac{L_{MTBCS}}{L}$	$\Delta t$
7.5	16	Tab. II [3]	$1.33 \times 10^2$	1.18	0.12	0.81	0.97	0.17	0.59	0.81	0.2	1.20	0.96	0.21
18	37	Dolph	1.04	0.65	1.44	1.57	1.00	0.26	2.81	0.65	1.5	1.57	1.00	1.60
7.0	14	Tab. III [3]	0.52	1.47	0.018	0.65	0.98	0.52	0.22	0.73	0.93	1.38	0.98	0.45

creasing the number of radiating elements when  $\beta_1 > 10^4$  [Fig. 4(c)]. Larger values of  $\beta_2$  yield more sparsely filled layouts, while smaller priors provide higher accuracies [Fig. 4(d)]. Consequently, the ranges for the scale priors have been set to  $\beta_1 \in [10^2, 10^4]$  and  $\beta_2 \in [5 \times 10^1, 5 \times 10^2]$ , respectively.

As far as the lattice grid is concerned, Fig. 4(e) shows that the matching accuracy is quite stable if  $N \gtrsim 2L_{UNI}/\lambda$ , while larger/smaller  $N$  values result in a sharp increase of  $P_{MTBCS}/\xi$ . This is mainly caused by the increased numerical complexity of the problem at hand since its size grows with  $N$ . A trade-off value within  $N \in [5L_{UNI}/\lambda, 50L_{UNI}/\lambda]$  is then suggested.

The obtained tradeoff margins range from a 1 : 1.2 ratio [for  $K$ —Fig. 4(a)] to a 1 : 100 ratio [for  $\beta_1$  and  $\sigma^2$ —Fig. 4(b) and (c)]. Such a behavior, caused by the different physical meaning of each parameter (see discussion above), does not actually represent a big issue for the proposed design methodology. In fact, quite wide ranges exist for which the method performances are almost constant. Furthermore, the  $MT$ -based  $BCS$  exhibits a “smoother” dependence on its control parameters than the single-task  $BCS$  approach. Indeed, unlike the  $BCS$ [18],  $\xi$  generally exhibits nearly monotone behavior versus control parameters [e.g., Fig. 4(a)–(e)] and  $P_{MTBCS}$  presents reduced oscillations given very large parameter variations [e.g., Fig. 4(c)]. Thus  $MT - BCS$  provides better stability and robustness than  $BCS$  for any reference pattern or aperture.

### B. $MT - BCS$ Assessment

For numerical assessment, we consider both unconstrained (Section III-B-I) and constrained problems (Section III-B-II), where forbidden regions are defined in the pattern region [Section I] or on the array geometry [Section II]. Concerning the unconstrained syntheses, the analysis aims at performing a consistency check to assess the reliability of the  $MT - BCS$  in dealing with problems also manageable by the original  $BCS$  approach [18] [Section I] and successively detailing the  $MT - BCS$  performance applied to the synthesis of arbitrary unconstrained patterns also in comparison with state-of-the-art methods [Sections II–III].

#### 1) Unconstrained Synthesis:

i) *Consistency Check (Hermitian Patterns)*<sup>2</sup> In order to compare  $BCS$  and  $MT - BCS$  approaches when dealing with Hermitian patterns, let us consider a  $L = 18\lambda$  equi-ripple reference pattern ( $PSL = -14.45$  dB) synthesized with the uniform array design method in [3] ( $P_{UNI} = 37$ ). The plots of the Pareto fronts in the  $\xi - P$  plane indicate that, as expected, the two solutions’ results are very close over a range of  $P$  [Fig. 5(a)]. The optimal trade-offs [ $P_{MTBCS} = P_{BCS} = 24$ ,

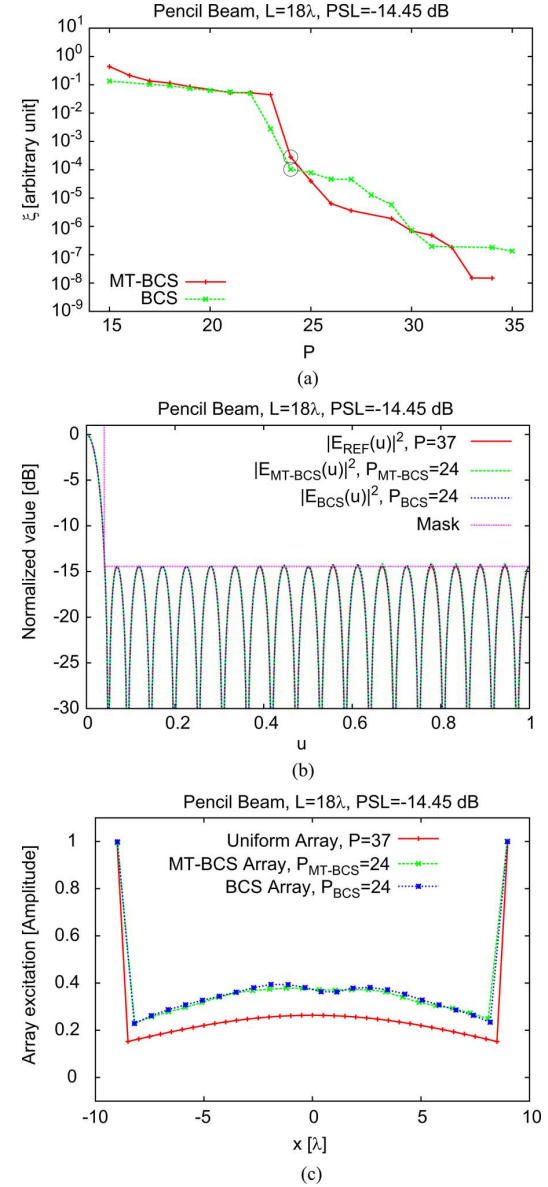


Fig. 5. Consistency Check (Hermitian Pattern Synthesis:  $L = 18\lambda$ ,  $P_{REF} = P_{UNI} = 37$ ,  $PSL = -14.45$  dB)— $MT - BCS$  vs.  $BCS$  (a) Pareto fronts in the  $(\xi, P)$  plane (b) optimal trade-off power patterns, and (c) the corresponding excitation amplitudes.

$\xi \approx \xi_{th}$ —Fig. 5(a)] turn out similar in both patterns [Fig. 5(b)] and weights [Fig. 5(c)] as also confirmed by the figures of merit in Table I, notwithstanding the different synthesis processes. Both  $BCS$  and  $MT - BCS$  behave similarly with Hermitian reference patterns, since a key difference between  $BCS$  and  $MT - BCS$  is the numerical handling of the relation between the real and imaginary parts of the array weights, and  $\mathcal{I}(v_p) = 0$  ( $p = 1, \dots, P$ ) when the reference pattern is Hermitian [Fig. 5(b)].

<sup>2</sup>Hermitian Pattern means symmetric pattern amplitude and anti-symmetric pattern phase that can also be generated by only real array weights.

TABLE II  
UNCONSTRAINED SYNTHESIS(HERMITIAN PATTERN:  $P_{REF} = P_{UNI}$  [17])—ARRAY PERFORMANCE INDEXES

	$L [\lambda]$	$PSL [\text{dB}]$	$P$	$\xi$	$\frac{P}{P_{REF}}$	$\frac{\Delta L_{min}}{\lambda/2}$	$\frac{\Delta L}{\lambda/2}$	$\frac{L}{L_{REF}}$	$\Delta t$
[17]	19.50	-5.10	16	—	1.00	2.00	2.60	1.00	-
<i>BCS</i>	19.50	-5.10	16	$2.34 \times 10^{-7}$	1.00	2.00	2.60	1.00	0.48
<i>MT—BCS</i>	19.50	-5.10	16	$2.14 \times 10^{-8}$	1.00	2.00	2.60	1.00	0.30
[17]	25.00	-14.45	24	—	1.00	1.00	2.17	1.00	-
<i>BCS</i>	24.94	-13.63	20	$3.58 \times 10^{-3}$	0.83	0.95	2.62	1.00	1.11
<i>MT—BCS</i>	24.95	-13.30	20	$4.3 \times 10^{-3}$	0.83	1.00	2.62	1.00	2.23
[17]	50.00	-14.45	25	—	1.00	1.00	4.17	1.00	-
<i>BCS</i>	32.99	-11.70	22	$2.06 \times 10^{-2}$	0.84	0.50	4.02	0.76	5.04
<i>MT—BCS</i>	32.99	-12.92	21	$7.19 \times 10^{-3}$	0.84	1.00	3.30	0.76	4.52

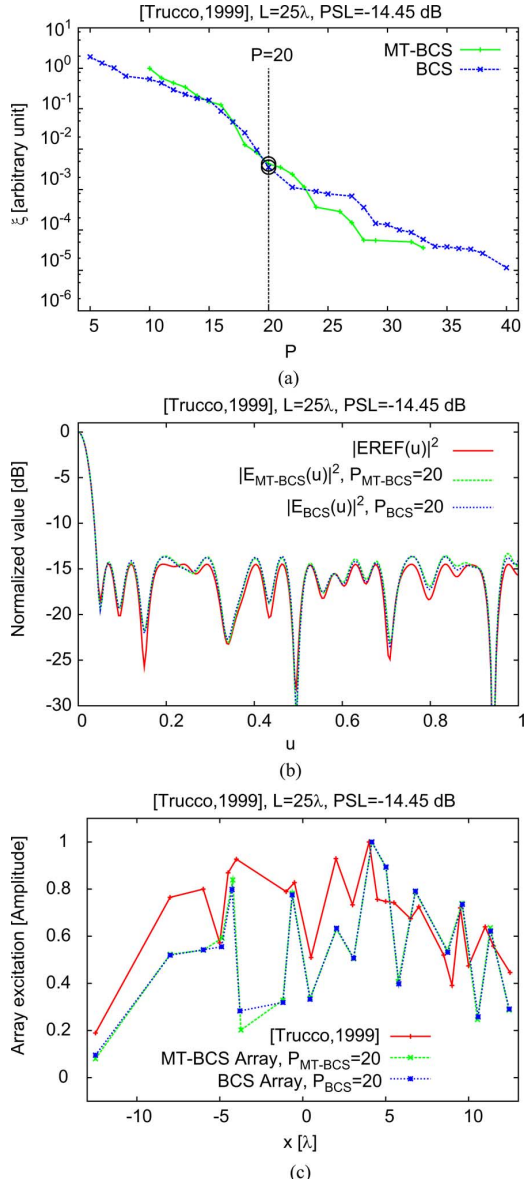


Fig. 6. Consistency Check (Hermitian Pattern Synthesis:  $L = 25\lambda$ ,  $P_{REF} = 24$ ,  $PSL = -14.45 \text{ dB}$  [17])—*MT—BCS* vs. *BCS* (a) Pareto fronts in the  $(\xi, P)$  plane (b) optimal trade-off power patterns, and (c) the corresponding excitations.

To further assess that such a behavior is due to the symmetry properties of the pattern at hand, the next numerical experiment is concerned with a set of Hermitian patterns derived from [17]. The results of the synthesis of the three layouts with

$L = \{19.5 \lambda, 25 \lambda, 50 \lambda\}$  are presented in Table II and compared with the sparse arrangements generated by a stochastic methodology based on simulated-annealing (*SA*) [17]. As it can be observed, the *BCS* and *MT—BCS* procedures achieve similar performances for each qualitative index (e.g., the matching accuracy and the array aperture) with an element saving equal or better than that of the stochastic approach (Table II). This is also visually confirmed by the plots in Fig. 6 related to the representative example characterized by  $L = 25\lambda$  and  $PSL = -14.45 \text{ dB}$  [17]. With reference to the layout with  $P_{BCS} = P_{MTBCS} = 20$  elements, it turns out that an acceptable fidelity [ $\xi \leq 4.3 \times 10^{-3}$ —Fig. 6(b)] is yielded by both *BCS*-based methods despite the reduction of the array elements with respect to the *SA*-optimized sparse solution ( $P_{SA} = 24$ ). The similarities are not limited to the patterns, but as expected, are apparent also in the distribution of the real array coefficients [Fig. 6(c)].

ii) *Symmetric Power Patterns*: Unlike Hermitian patterns, *BCS* and *MT—BCS* syntheses are expected to differ when only the reference power pattern is symmetric. The results from the synthesis of a non-Hermitian flat-top array ( $P_{UNI} = 14$ —[3]) with symmetric power pattern [Fig. 7(a)] and asymmetric phase distribution [Fig. 7(b)] reveal the enhanced effectiveness of the *MT* procedure, which is due to its improved accuracy in modelling the statistical relations between the (non-negligible) real and imaginary parts of the array weights. As far as the optimal *BCS*-based trade-off solutions are concerned, it turns out that there is a halving of the array elements [ $P_{BCS} = 22$  vs.  $P_{MTBCS} = 11$ —Table I] along with similar matching accuracies [ $\xi_{BCS} = 0.52 \times 10^{-4}$  vs.  $\xi_{MTBCS} = 0.22 \times 10^{-4}$ —Table I]. This latter is mainly due to the intrinsic limitation of the *BCS* approach to deal with the two components of the array excitations as correlated unknowns [(6)]. Indeed, several *BCS* weights turn out either purely real or purely imaginary [ $\angle v_p|_{BCS} \in \{0, \pm\pi/2, \pm\pi\}$ —Fig. 7(d)] unlike the *MT—BCS* coefficients.

iii) *Asymmetric Power Patterns*: The improvements of the *MT—BCS* approach are expected to be even more impressive when asymmetric patterns are at hand. In order to analyze such a case, the next example deals with the synthesis of a  $L = 7.5\lambda$  cosecant pattern from [3] [ $P_{UNI} = 16$ , Fig. 8(b)]. The Pareto *BCS* solutions in the  $\xi - P$  plane [Fig. 8(a)] clearly indicate that the multi-task procedure is far more efficient than the single-task one. Indeed, the *MT—BCS* yields sparser layouts for a fixed  $\xi$  threshold [e.g.,  $P_{MTBCS}/P_{BCS} = 0.68$  when  $\xi \approx \xi_{th}$ —Fig. 8(a)], and a higher accuracy for a given  $P$  [e.g.,  $\xi_{MTBCS}/\xi_{BCS} \approx 8.0 \times 10^{-5}$  when  $P = 15$ —Fig. 8(a)]. As

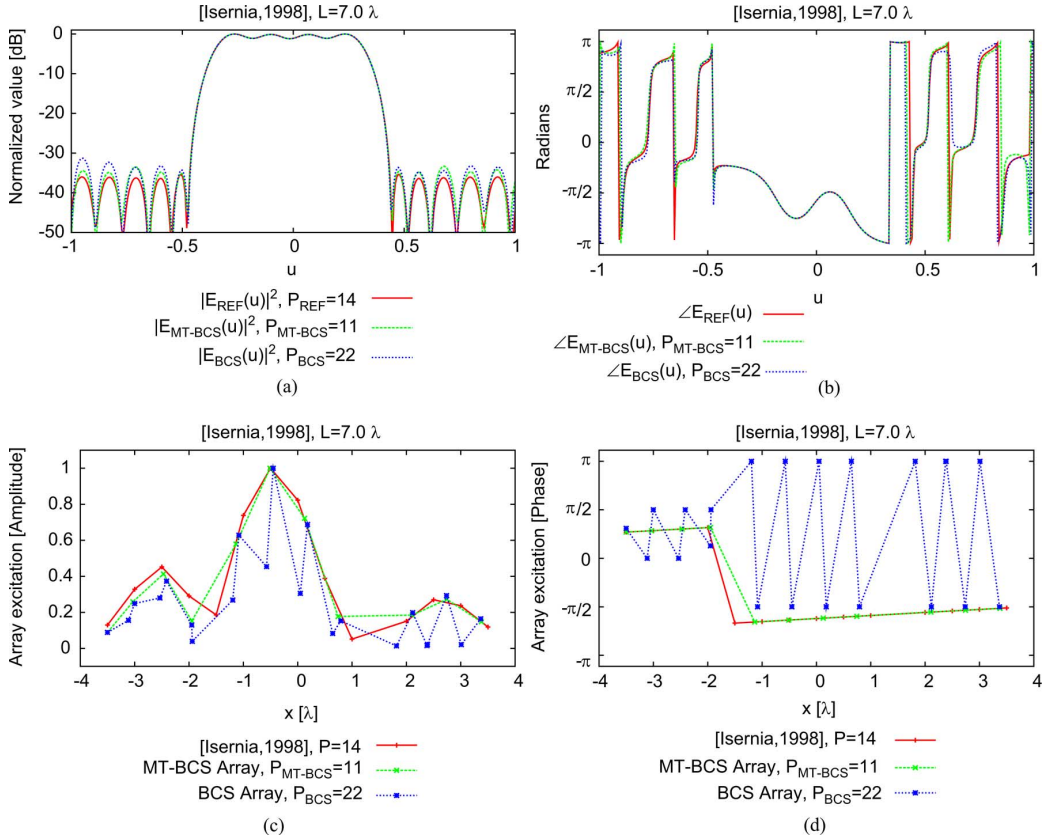


Fig. 7. Comparative Assessment (Symmetric Power Pattern Synthesis): “Flat top,”  $L = 7\lambda$ ,  $P_{REF} = P_{UNI} = 14$  [3]—Pattern amplitudes (a), pattern phases (b), excitation amplitudes (c), excitation phases (d) of the uniform array [3]] and of the optimal trade-off  $BCS$  and  $MT - BCS$  layouts.

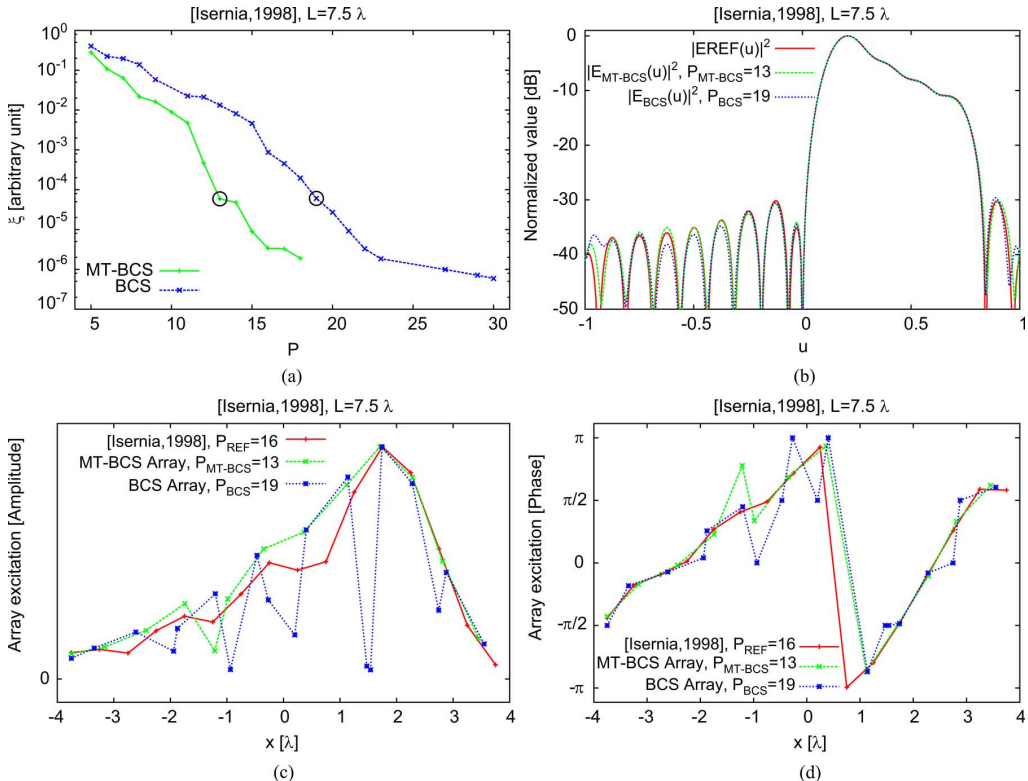


Fig. 8. Comparative Assessment (Asymmetric Power Pattern Synthesis): “Cosecant,”  $L = 7.5\lambda$ ,  $P_{REF} = P_{UNI} = 16$  [3]—(a)  $MT - BCS$  and  $BCS$  Pareto fronts in the  $(\xi, P)$  plane. Power patterns (b), excitation amplitudes (c), and excitation phases (d) of the uniform array [3] and of the optimal trade-off  $BCS$  and  $MT - BCS$  layouts.

TABLE III  
UNCONSTRAINED SYNTHESIS (ASYMMETRIC PATTERN: “COSECANT,”  $P_{REF} = P_{UNI}$  [3])—ARRAY PERFORMANCE INDEXES

Reference Pattern			BCS						MT – BCS					
$L [\lambda]$	$PSL$	$P_{UNI}$	$\xi [\times 10^{-4}]$	$P_{BCS}/P_{UNI}$	$\Delta L_{min}/\lambda/2$	$\Delta L/\lambda/2$	$L_{BCS}/L_{UNI}$	$\Delta t$	$\xi [\times 10^{-4}]$	$P_{MTBCS}/P_{UNI}$	$\Delta L_{min}/\lambda/2$	$\Delta L/\lambda/2$	$L_{MTBCS}/L_{UNI}$	$\Delta t$
12	-20	25	3.00	1.28	0.048	0.77	1.00	0.29	0.53	0.76	0.74	1.33	1.00	7.73
12	-30	25	2.86	1.28	0.048	0.77	1.00	0.38	0.38	0.84	0.51	1.2	1.00	1.39
12	-40	25	0.24	1.28	0.49	0.77	1.00	0.23	0.11	0.84	0.72	1.2	1.00	0.87
14.5	-20	30	0.48	1.2	0.59	0.83	1.00	0.23	0.46	0.80	0.49	1.26	1.00	0.56
14.5	-30	30	1.29	1.23	0.058	0.8	0.99	0.44	1.47	0.80	0.63	1.26	1.00	2.85
14.5	-40	30	0.96	1.47	0.33	0.67	1.00	0.25	0.81	0.77	0.40	1.28	0.98	3.82
19.5	-20	40	3.75	1.3	0.67	0.75	0.98	0.24	2.27	0.78	0.54	1.30	1.00	6.19
19.5	-30	40	1.29	1.43	0.31	0.70	1.00	1.30	0.80	0.78	0.19	1.30	1.00	6.99
19.5	-40	40	0.83	1.35	0.39	0.74	1.00	0.36	0.44	0.78	0.52	1.30	1.00	4.38

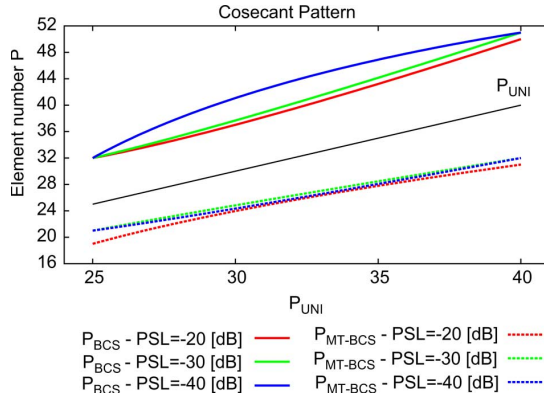


Fig. 9. Comparative Assessment (Asymmetric Power Pattern Synthesis: “Cosecant,”  $P_{REF} = P_{UNI}$  [3])—Plot of  $P$  vs.  $P_{UNI}$  for different values of the  $PSL$  [dB] of the reference pattern.

an illustrative example, the patterns [Fig. 8(b)] and the array coefficients [Fig. 8(c)–(d)] of the representative solutions circled in Fig. 8(a) [ $P_{BCS} = 19$  vs.  $P_{MTBCS} = 13$ ] are shown. As far as the array layouts are concerned, it is worth noticing that an element saving of  $\approx 20\%$  ( $P_{MTBCS}/P_{UNI} = 0.81$ ) and an aperture reduction of  $\approx 4\%$  ( $L_{MTBCS}/L_{UNI} = 0.96$ ) with respect to the uniform solution are obtained by the  $MT – BCS$  without compromising the pattern matching accuracy (Table I), while the  $BCS$  fails in reducing the array elements ( $P_{MTBCS}/P_{UNI} = 1.18$ ). Moreover, the behavior of the array excitations over the aperture confirms that the non-uniform  $MT – BCS$  distribution follows the uniform one since the pattern matching refers to the complex reference pattern and not only to the power pattern, thus constraining both amplitudes and phases of the array coefficients.

To provide a more exhaustive comparison of the  $BCS$  methodologies, the results of an extensive analysis on asymmetric “cosecant” reference patterns with constant sidelobes are presented. More specifically, the reference patterns have been chosen such that  $L \in \{12\lambda, 19.5\lambda\}$  (i.e.,  $P_{UNI} \in \{25, 40\}$ ) and  $PSL = \{-20 \text{ dB}, -30 \text{ dB}, -40 \text{ dB}\}$ . The plots of  $P$  for the optimal (i.e.,  $\xi \sim \xi_{th}$ ) trade-off  $BCS$  and  $MT – BCS$  layouts are shown in Fig. 9 as a function of  $P_{UNI}$ . By observing the case of the reference pattern with  $PSL = -20 \text{ dB}$ , the  $MT$  technique always outperforms the single-task method with significantly sparser solutions ( $P_{MTBCS}/P_{BCS} \in [0.59, 0.66]$ —Table III). This holds true also when lowering the sidelobe level (Fig. 9). On the other hand, although more array elements are necessary as

$P_{UNI}$  increases, the  $MT – BCS$  always enables a reduction of the array elements with respect to the uniform architectures (Fig. 9— $P_{MTBCS} < P_{UNI}$ ), while the condition  $P_{BCS} > P_{UNI}$  is mandatory for the  $BCS$  to reach the accuracy threshold  $\xi \sim 10^{-4}$  [ $P_{MTBCS}/P_{UNI} \in [0.76, 0.84]$  vs.  $P_{BCS}/P_{UNI} = 1.28$ —Table III]. The effectiveness of the  $MT – BCS$  to reduce the number of elements in the array arrangement is pictorially highlighted in the representative example analyzed in Fig. 10 ( $PSL = -40 \text{ dB}$ ). Whatever the matching accuracy, the  $MT – BCS$  patterns exhibit a higher sparseness [Fig. 10(a)–(f)] than the  $BCS$ . Furthermore, the pattern matching of the  $MT – BCS$  solution is always better for a given value of  $P$  [Fig. 10(a), (c), (e)].

The  $BCS$  approach is usually faster<sup>3</sup> than the multi-task procedure, although both methods do not require heavy computations [ $\Delta t \leq 8 \text{ s}$ —Table III]. This is expected since neglecting the relationships between real and imaginary parts of the array excitations (see Section II) simplifies the problem, but significantly degrades the synthesis performance with complex layouts.

As for the state-of-the-art comparisons, let us refer to recently introduced approaches based on the Matrix Pencil Method (*MPM*) [11], [30], [31], [44]. Such a choice is mainly due to their effectiveness and numerical efficiency usually outperforming other sparse-synthesis methods in terms of convergence speed, reliability, and accuracy [11], [30], [31].

The first set of comparisons is concerned with the benchmark case in [43]. The synthesis results are reported in Fig. 11(a)–(b) and quantitatively compared in Table IV. With reference to the  $(\xi, P)$ -plane [Fig. 11(a)], the stand-alone matrix pencil method [30] is, as expected, significantly less accurate ( $P = 19$ :  $\xi_{MPM} = 1.43 \times 10^{-1}$  [Fig. 11(b)] vs.  $\xi_{MTBCS} = 3.53 \times 10^{-3}$ —Table IV) than the sub-optimal (i.e.,  $\xi > \xi_{th}$ )  $MT – BCS$  because of the shaped-beam reference pattern [11], while the hybrid *TABU – MPM* (*TMPM*) [44] reaches a comparable pattern matching ( $P = 19$ :  $\xi_{MPM-TABU} = 3.21 \times 10^{-3}$ —Table IV) although requiring a non-negligible computational burden [44] because of the *TABU*-based stochastic optimization in the second step of the hybrid procedure.

Concerning the so-called forward-backward version of the matrix pencil method (*FBMPM*) [31], the results in Fig. 11(c)–(f) derived from [45], [46] (also discussed in [31]) point out that the *FBMPM* exhibits performance close

<sup>3</sup>In all cases, the synthesis time  $\Delta t$  refers to the execution of the Matlab code on a single core laptop running at 2.16 GHz.

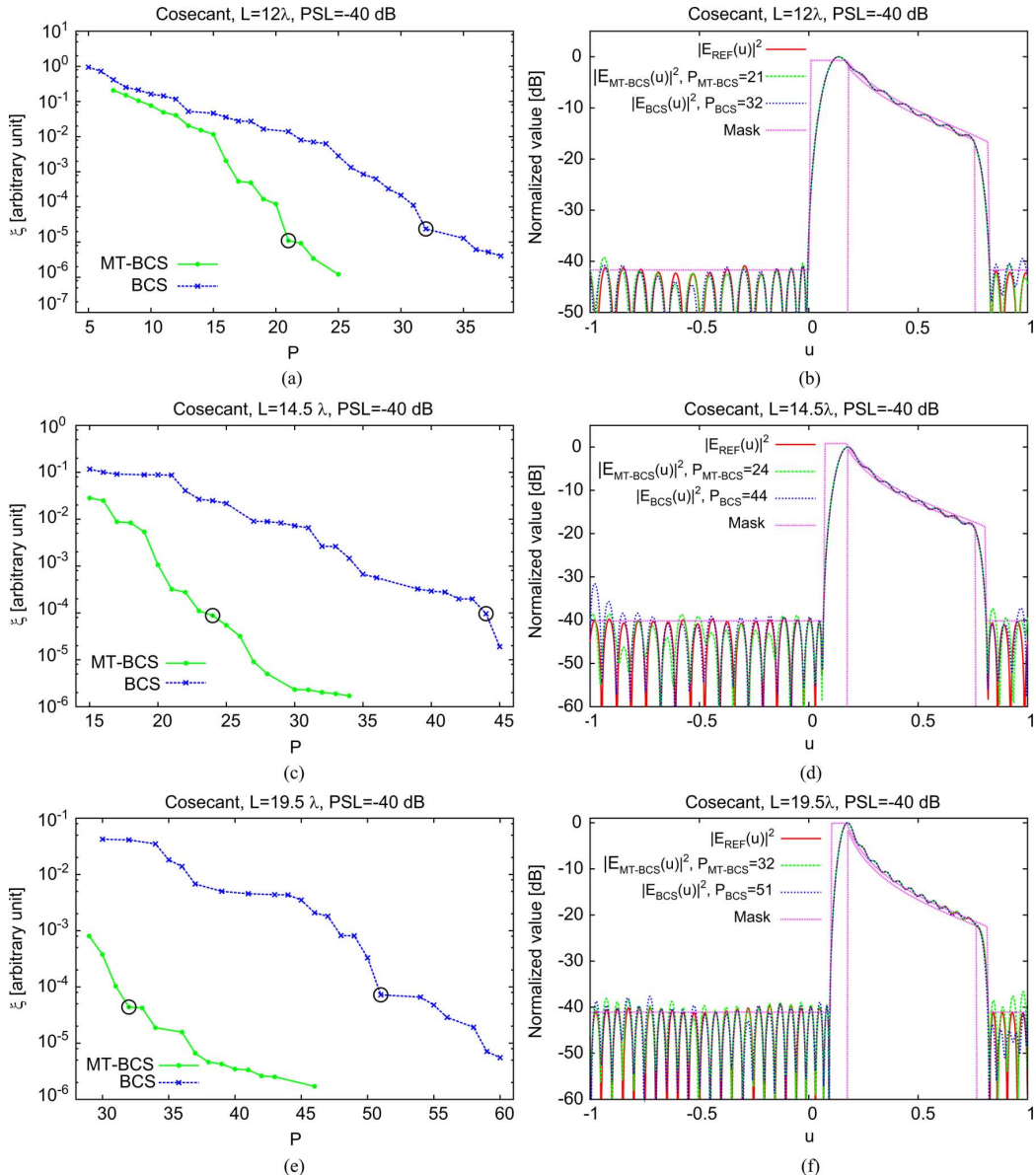


Fig. 10. Comparative Assessment (Asymmetric Power Pattern Synthesis: “Cosecant,”  $P_{REF} = P_{UNI}$ ,  $PSL = -40$  dB [3])—BCS and  $MT - BCS$  Pareto fronts in the  $(\xi, P)$  plane (left column), power patterns of the reference uniform array [3] and of the optimal trade-off BCS and  $MT - BCS$  solutions (right column) (a),(b)  $L = 12\lambda$  ( $P_{UNI} = 25$ ) (c),(d)  $L = 14.5\lambda$  ( $P_{UNI} = 30$ ), and (e),(f)  $L = 19.5\lambda$  ( $P_{UNI} = 40$ ).

to that of the  $MT - BCS$  when dealing with shaped-pattern problems [e.g.,  $P = 13$ :  $\xi_{FBMPM} = 8.09 \times 10^{-5}$  vs.  $\xi_{MTBCS} = 5.32 \times 10^{-5}$ —Table V and Fig. 11(c);  $P = 15$ :  $\xi_{FBMPM} = 4.94 \times 10^{-5}$  vs.  $\xi_{MTBCS} = 1.68 \times 10^{-4}$ —Table VI and Fig. 11(e)].

However, it cannot be neglected that the MPM (and, consequently, the FBMPM) can present some numerical instabilities (or no convergence) as it was pointed out in [11], [15] and confirmed by the synthesis results of the “cosecant” pattern with  $PSL = -40$  dB generated by the uniform aperture  $L = 14.5\lambda$  (Fig. 13) as well as for the test case in [47] (Fig. 12). Unlike the BCS-based approaches, the fitting with the reference pattern of the FBMPM<sup>4</sup>,  $\xi_{FBMPM}$ , does not monotonically improve

<sup>4</sup>A MATLAB implementation of the FBMPM (based on the mpencil function <http://www.mathworks.se/matlabcentral/index.html>) have been used assuming the parameters suggested in [31] for the following numerical tests.

as  $P$  grows [Figs. 12(a) and 13(a)]. For example [Fig. 12(a)], the  $MT - BCS$  reaches the matching threshold  $\xi \sim \xi_{th}$  (i.e.,  $\xi_{MTBCS}|_{P=16} = 9.27 \times 10^{-5}$ —Table VII) just adding an element to the array with  $P_{MTBCS} = 15$ , while the FBMPM accuracy worsens when moving from  $P_{FBMPM} = 14$  to  $P_{FBMPM} = 16$  ( $\xi_{FBMPM}|_{P=14} = 8.50 \times 10^{-4}$  vs.  $\xi_{FBMPM}|_{P=16} = 6.79 \times 10^{-3}$ ). Therefore, the  $MT - BCS$  faithfully reconstructs the reference pattern [Fig. 12(b)] reducing the uniform array elements of 1/5 unlike the FBMPM that does not provide the same accuracy (i.e.,  $\xi \leq 10^{-4}$ ) unless using more radiators ( $P_{FBMPM} = 19 \rightarrow \xi_{FBMPM}|_{P=19} = 4.60 \times 10^{-6}$ ). Similar outcomes can be drawn from the test case in Fig. 13 (Table VII) that allows us to point out also another interesting feature of the BCS-based approaches. By observing the FBMPM arrangement in Fig. 13(c), it turns out that the minimum inter-element

TABLE IV

UNCONSTRAINED SYNTHESIS (ASYMMETRIC PATTERN: “COSECANT,”  $L = 14.5\lambda$ ,  $P_{REF} = P_{UNI} = 30$  [43])—ARRAY PERFORMANCE INDEXES

				<i>Optimal Tradeoff</i> ( $\xi \leq \xi_{th}$ )		<i>Sub-Optimal Tradeoff</i> ( $\xi > \xi_{th}$ )	
	Uniform [43]	MPM [44]	TMPM [44]	BCS	MT – BCS	BCS	MT – BCS
$L[\lambda]$	14.5	14.47	14.14	14.5	14.5	11.28	13.00
$P$	30	19	19	35	24	20	19
$\frac{P}{P_{UNI}}$	—	0.63	0.63	1.17	0.8	0.66	0.63
$\frac{\Delta L_{min}}{\Delta L_{UNI}}$	—	1.15	1.20	0.29	0.058	0.29	0.075
$\frac{\Delta L}{\Delta L_{UNI}}$	—	1.61	1.57	0.85	1.26	1.19	1.45
$\frac{L}{L_{UNI}}$	—	1	0.98	1.00	1.00	0.78	0.90
$t[s]$	—	—	—	0.24	0.53	0.22	0.97
$\xi$	—	$1.43 \times 10^{-1}$	$3.21 \times 10^{-3}$	$9.85 \times 10^{-5}$	$8.15 \times 10^{-5}$	$3.71 \times 10^{-2}$	$3.53 \times 10^{-3}$

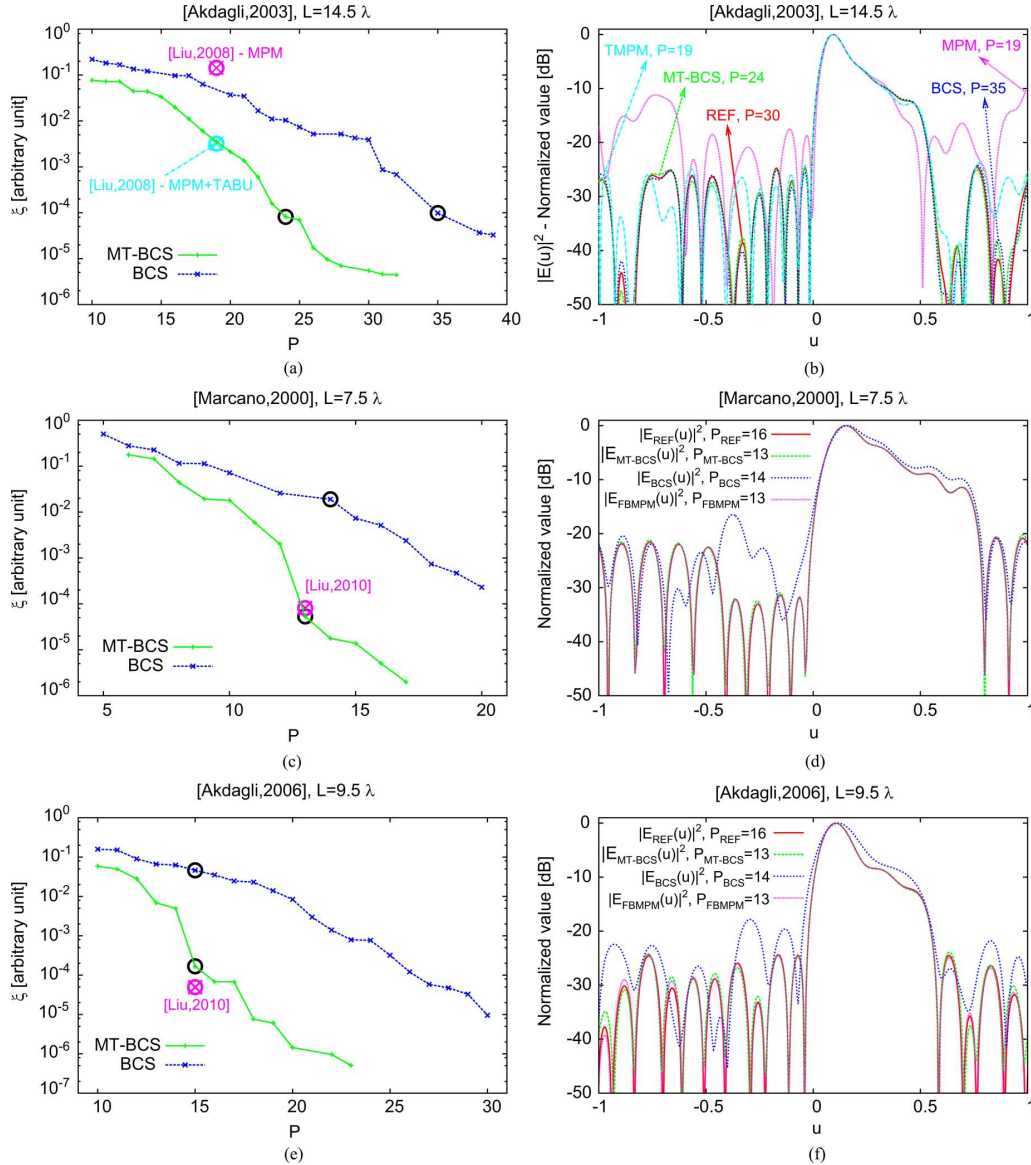


Fig. 11. Comparative Assessment (Asymmetric Power Pattern Synthesis: “Cosecant,”  $P_{REF} = P_{UNI}$ )—Representative points in the  $(\xi, P)$  plane of the BCS and MT – BCS Pareto fronts and of the MPM-based methods (left column), power patterns of the reference uniform array, the MPM-based methods, and the optimal trade-off BCS and MT – BCS solutions (right column) (a),(b)  $L = 14.5\lambda$  ( $P_{UNI} = 30$ ) [43] (c),(d)  $L = 7.5\lambda$  ( $P_{UNI} = 16$ ) [45], and (e),(f)  $L = 9.5\lambda$  ( $P_{UNI} = 20$ ) [46].

spacing is very small and equal to  $\Delta L_{min} = 1.62 \times 10^{-3}\lambda$  (Table VII). On the contrary, the BCS rationale with the choice of the candidate locations for the array elements,  $d$ , gives the user the possibility to *a-priori* impose the lower bound for the distance between two adjacent elements. As for the *CPU*-time,

the indexes in Table VII indicate that the synthesis time for the MT – BCS and the FBMPM is generally of the same order in magnitude (e.g.,  $\Delta t_{FBMPM} = 7.83 \times 10^{-1}$ [s] vs.  $\Delta t_{MTBCS} = 6.70 \times 10^{-1}$ [s]).

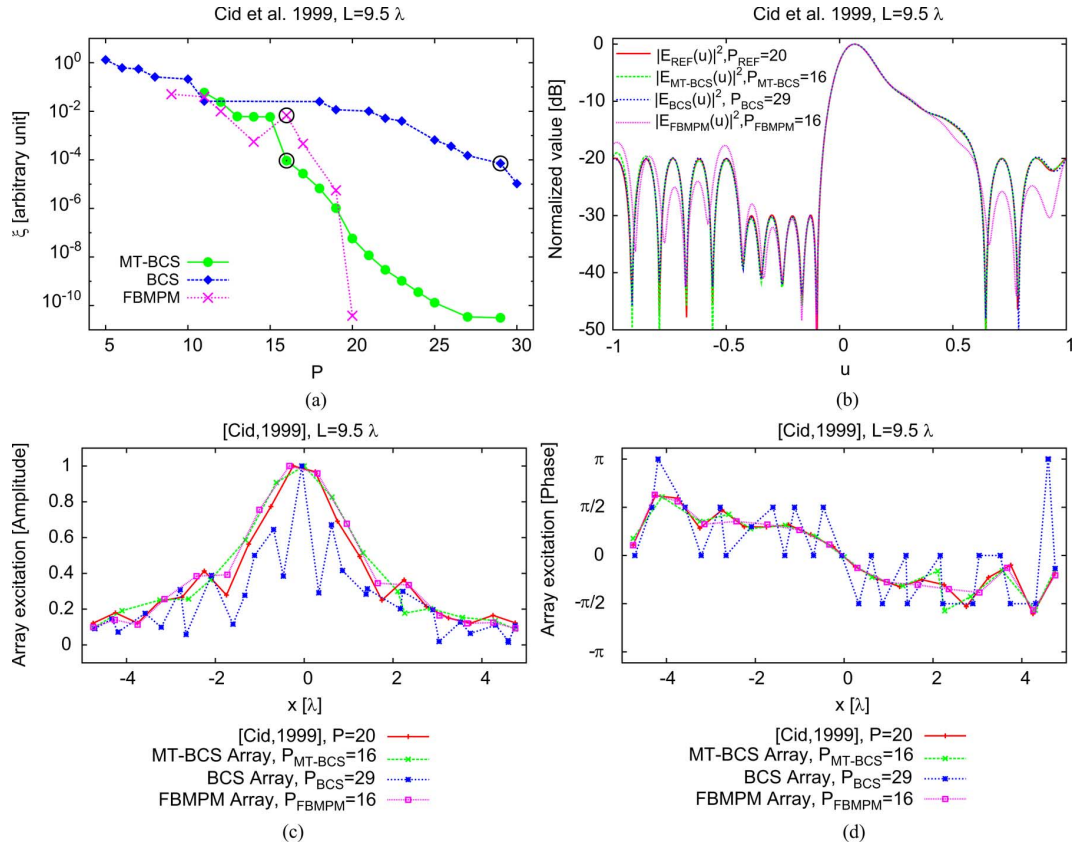


Fig. 12. Comparative Assessment (Asymmetric Power Pattern Synthesis: “Shaped Cosecant,”  $P_{REF} = P_{UNI} = 20$ ,  $L = 9.5\lambda$  [47])—FBMPPM, BCS, and MT—BCS solutions (a) Pareto fronts in the  $(\xi, P)$  plane (b) power patterns (c) excitation amplitudes, and excitation phases (d).

TABLE V  
UNCONSTRAINED SYNTHESIS (ASYMMETRIC PATTERN: “COSECANT,”  $L = 7.5\lambda$ ,  $P_{REF} = P_{UNI} = 16$  [45])—ARRAY PERFORMANCE INDEXES

	[45]	FBMPPM [31]	BCS	MT—BCS
$L[\lambda]$	7.5	7.51	7.50	7.46
$P$	16	13	14	13
$\frac{P}{P_{UNI}}$	—	0.81	0.88	0.81
$\frac{\Delta L_{min}}{\Delta L_{UNI}}$	—	1.06	0.042	0.74
$\frac{\Delta L}{\Delta L_{UNI}}$	—	1.25	1.15	1.24
$\frac{L}{L_{UNI}}$	—	1	1	1
$t[s]$	—	—	0.16	1.00
$\xi$	—	$8.09 \times 10^{-5}$	$1.89 \times 10^{-2}$	$5.32 \times 10^{-5}$

2) *Constrained Synthesis:* Previous discussions gave some insights about the efficiency of the MT—BCS in dealing with shaped reference patterns as well as about its advances in terms of element sparseness, matching accuracy, final layout properties, and numerical efficiency over the standard BCS or in comparison with reference state-of-the-art methodologies. The final set of experiments, concerned with an equi-ripple ( $PSL = -30$  dB) cosecant reference pattern generated by a uniform aperture of  $L = 19.5\lambda$ , points out the flexibility of the BCS-based methodology to handle constrained sparse-array syntheses. Performing constrained sparse synthesis is not a trivial task for a wide range of state-of-the-art methods, except for optimization methods which, however, usually involve heavy computations when high-dimension solution spaces are at hand.

TABLE VI  
UNCONSTRAINED SYNTHESIS (ASYMMETRIC PATTERN: “COSECANT,”  $L = 9.5\lambda$ ,  $P_{REF} = P_{UNI} = 20$  [46])—ARRAY PERFORMANCE INDEXES

	[46]	FBMPPM [31]	BCS	MT—BCS
$L[\lambda]$	9.5	9.375	9.5	9.34
$P$	20	15	15	15
$\frac{P}{P_{UNI}}$	—	0.75	0.75	0.75
$\frac{\Delta L_{min}}{\Delta L_{UNI}}$	—	1.23	0.39	0.97
$\frac{\Delta L}{\Delta L_{UNI}}$	—	1.34	1.36	1.35
$\frac{L}{L_{UNI}}$	—	0.99	1.00	0.98
$t[s]$	—	—	0.18	0.98
$\xi$	—	$4.94 \times 10^{-5}$	$4.62 \times 10^{-2}$	$1.68 \times 10^{-4}$

i) *Pattern Constraints:* The first test case has been designed by limiting the reference pattern samples  $F_{REF}(u_k)$  to the angular region  $u \in (-0.7, 0.9)$  [i.e.,  $u_k \notin \{-1, -0.7\} \cup [0.9, 1]\} k = 1, \dots, K$ ]. As expected, the optimal trade-off MT—BCS and BCS patterns faithfully match the reference pattern only within the constrained region  $[\xi_{MTBCS}]_{P=29} = 2.35 \times 10^{-5}$  vs.  $\xi_{BCS}|_{P=44} = 4.96 \times 10^{-5}$ —Fig. 14(a)] guaranteeing a reduction, more significant for the BCS even though still  $P_{BCS}^{unc} = 44 > P_{UNI} = 40$ , of the element number with respect to the full-constrained case ( $P^{con}/P^{unc}|_{MTBCS} = 1.07$  and  $P^{con}/P^{unc}|_{BCS} = 1.29$ ).

ii) *Geometry Constraints:* The last cases model aperture blockage constraints within the BCS syntheses by setting forbidden regions for the radiating elements

TABLE VII  
UNCONSTRAINED SYNTHESIS (ASYMMETRIC PATTERN: “COSECANT.”  $P_{REF} = P_{UNI}$ )—ARRAY PERFORMANCE INDEXES

	[47] - $P_{UNI} = 20, L_{UNI} = 9.5\lambda$			$P_{UNI} = 30, L_{UNI} = 14.5\lambda$		
	$FBMPM$	$BCS$	$MT - BCS$	$FBMPM$	$BCS$	$MT - BCS$
$L [\lambda]$	9.5	9.46	9.5	14.5	14.5	14.5
$P$	16	29	16	24	44	24
$\frac{P}{P_{UNI}}$	0.8	1.45	0.8	0.8	1.47	0.8
$\frac{\Delta L_{min}}{\Delta L_{UNI}}$	0.97	0.019	0.31	0.00324	0.34	0.45
$\frac{\Delta L}{\Delta L_{UNI}}$	1.27	0.68	1.27	1.26	0.67	1.26
$\frac{L}{L_{UNI}}$	1.00	1.00	1.00	1.00	1.00	1.00
$t [s]$	$7.83 \times 10^{-1}$	$5.58 \times 10^{-1}$	$6.70 \times 10^{-1}$	$9.61 \times 10^{-1}$	$2.5 \times 10^{-1}$	1.43
$\xi$	$6.79 \times 10^{-3}$	$7.14 \times 10^{-5}$	$9.27 \times 10^{-5}$	$3.98 \times 10^{-3}$	$9.62 \times 10^{-5}$	$7.93 \times 10^{-5}$

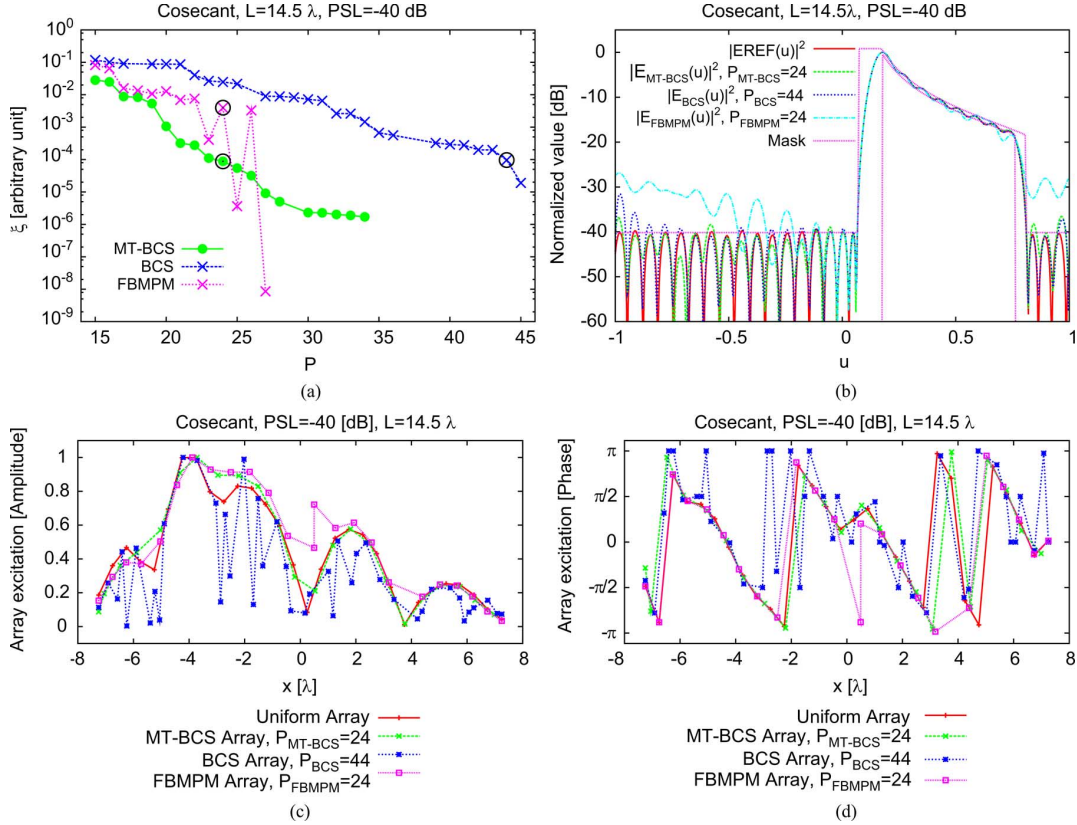


Fig. 13. Comparative Assessment (Asymmetric Power Pattern Synthesis: “Cosecant,”  $L = 19.5\lambda$ ,  $P_{REF} = P_{UNI} = 40$ ,  $PSL = -40$  dB [3])— $FBMPM$ ,  $BCS$ , and  $MT - BCS$  solutions (a) Pareto fronts in the  $(\xi, P)$  plane (b) power patterns (c) excitation amplitudes, and excitation phases (d).

[see Section II]. More specifically, two different scenarios have been investigated either defining symmetric ( $d_n \notin \{[-6\lambda, -5\lambda] \cup [5\lambda, 6\lambda]\}, n = 1, \dots, N$ ) or asymmetric ( $d_n \notin \{[-7\lambda, -6\lambda] \cup [3\lambda, 4\lambda]\}, n = 1, \dots, N$ ), forbidden regions. The plots of the optimal trade-off layouts and associated patterns (Fig. 15) show that both compressive-sampling procedures succeed in carefully reproducing the reference pattern [ $\xi_{MTBCS} = 1.01 \times 10^{-5}$  vs.  $\xi_{BCS} = 2.32 \times 10^{-5}$ —Fig. 15(a);  $\xi_{MTBCS} = 6.08 \times 10^{-5}$  vs.  $\xi_{BCS} = 9.68 \times 10^{-5}$ —Fig. 15(b)] while also complying with the geometrical constraints [Fig. 15(c)–(e) and Fig. 15(d)–(f)] despite the non-negligible aperture blockage ( $> 10\%$  in both cases). Furthermore, the  $MT - BCS$  technique confirms also in those scenarios its higher efficiency (than the  $BCS$ ) in minimizing the array elements [ $P_{BCS} = 63$  vs.  $P_{MTBCS} = 37$ —Fig. 15(c)–(e);  $P_{BCS} = 58$  vs.  $P_{MTBCS} = 34$ —Fig. 15(d)–(f)] also

with respect to the (unconstrained) uniform solution [ $P_{MTBCS}/P_{UNI} = 0.92$ —Fig. 15(c)–(e);  $P_{MTBCS}/P_{UNI} = 0.85$ —Fig. 15(d)–(f)]. Of course, the element saving turns out to be lower than that for the “unconstrained”  $BCS$ -based syntheses because of the greater complexity of the synthesis at hand [i.e.,  $P^{con}/P^{unco}|_{MTBCS} = 1.18$  and  $P^{con}/P^{unco}|_{BCS} = 1.09$  (symmetric forbidden region) and  $P^{con}/P^{unco}|_{MTBCS} = 1.09$  and  $P^{con}/P^{unco}|_{BCS} = 1.02$  (asymmetric forbidden region)].

#### IV. CONCLUSIONS

An innovative, flexible, and efficient complement to the existing approaches for the synthesis of sparse layouts with arbitrary radiation features has been proposed. The proposed method extends the range of applicability of the technique in [18] by considering a  $MT$  Bayesian methodology. Towards this end, the original pattern matching problem has been formulated

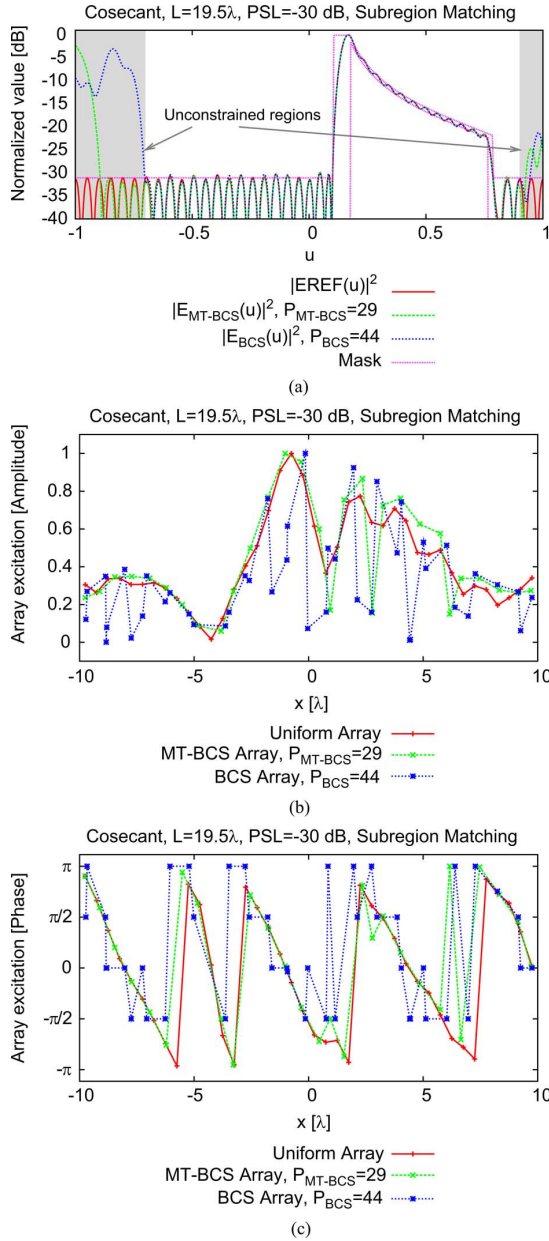


Fig. 14. Flexibility Check (Constrained Pattern Synthesis: “Cosecant,”  $L = 19.5\lambda$ ,  $PSL = -30$  dB,  $P_{REF} = P_{UNI} = 40$ ,  $u_k \notin \{[-1, -0.7] \cup [0.9, 1]\}$ )—Power patterns (a) and array coefficients (b) (c) of the optimal trade-off BCS and  $MT - BCS$  layouts.

in a Bayesian fashion within the framework of the sparseness constrained optimization and afterwards it has been solved by a suitable *RVM*-derived methodology. Selected results from an extensive numerical validation have been presented to provide an evaluation of the sensitivity of the  $MT - BCS$  method to its control parameters as well as on its accuracy, flexibility, and computational efficiency. Advantages and limitations of the proposed approach have been pointed out using comparisons with state-of-the-art approaches. In summary:

- the  $MT - BCS$  technique is simpler to calibrate than the single-task BCS approach thanks to its smoother dependency on the control parameters (Section III-A);
- the  $MT - BCS$  methodology outperforms the single-task BCS procedure since, generally, the BCS extension to

complex layouts often yields to (sub-optimal) arrangements mostly comprising purely-real and purely-imaginary excitations. As expected, BCS-based procedures provide very similar results when symmetric real layouts are at hand (Section III-B-I);

- on average, the  $MT - BCS$  guarantees an element saving with respect to ( $\lambda/2$ -spaced) uniform layouts of about  $P_{MTBGS}/P_{UNI} \in [0.65, 0.81]$  when complex- or real-valued symmetric patterns are at hand still providing an excellent pattern matching [ $\xi \lesssim 10^{-4}$ ];
- the  $MT - BCS$  favorably compares with state-of-the-art sparse array design procedures in terms of pattern matching accuracy, element saving, numerical efficiency, and stability;
- additional constraints on the radiation pattern and/or the geometrical features of the sparse array can be easily and efficiently dealt with (Section III-B-II).

In addition, other main and innovative contributions of this paper consist in the following methodological novelties:

- 1) an extension to the complex-valued synthesis problems of the BCS approach in [18];
- 2) an innovative and equivalent “fictitious” formulation of the complex-weight pattern matching problem for enabling the application of the  $MT - BCS$ ;
- 3) an innovative  $MT - BCS$  method for dealing with complex-valued sparseness constrained optimization by statistically correlating the real and the imaginary components of the sparse unknowns.

Future works, out-of-the-scope of the present paper, will be aimed at analyzing the mutual coupling effects between real elements in the sparse layouts as well as at taking into account in the synthesis process the presence of directive elements. Furthermore, the derivation of array processing algorithms (i.e., DOA-estimation [48] and adaptive beamforming [49] techniques) based on  $MT - BCS$  geometries will be the subject of future analyses aimed at exploiting and integrating the features of such a sparse arrangements in an effective and customized way.

## APPENDIX

### Derivation of (14)

To solve (13), the conditional probability  $\mathcal{P}(\mathbf{w}_H | \hat{\mathbf{F}}_H)$  is written according to the Bayes theorem, as

$$\mathcal{P}(\mathbf{w}_H | \hat{\mathbf{F}}_H) \triangleq \frac{\mathcal{P}(\hat{\mathbf{F}}_H | \mathbf{w}_H) \mathcal{P}(\mathbf{w}_H)}{\mathcal{P}(\hat{\mathbf{F}}_H)} \quad (16)$$

where  $\mathcal{P}(\hat{\mathbf{F}}_H | \mathbf{w}_H)$  is the “likelihood,” whereas  $\mathcal{P}(\hat{\mathbf{F}}_H)$  and  $\mathcal{P}(\mathbf{w}_H)$  are the priors of  $\hat{\mathbf{F}}_H$  and  $\mathbf{w}_H$ , respectively. Equation (16) is substituted in (13) to yield

$$\mathbf{w}_H^{MT-BCS} = \arg \left\{ \max_{\mathbf{w}_H} \left[ \frac{\mathcal{P}(\hat{\mathbf{F}}_H | \mathbf{w}_H) \mathcal{P}(\mathbf{w}_H)}{\mathcal{P}(\hat{\mathbf{F}}_H)} \right] \right\}. \quad (17)$$

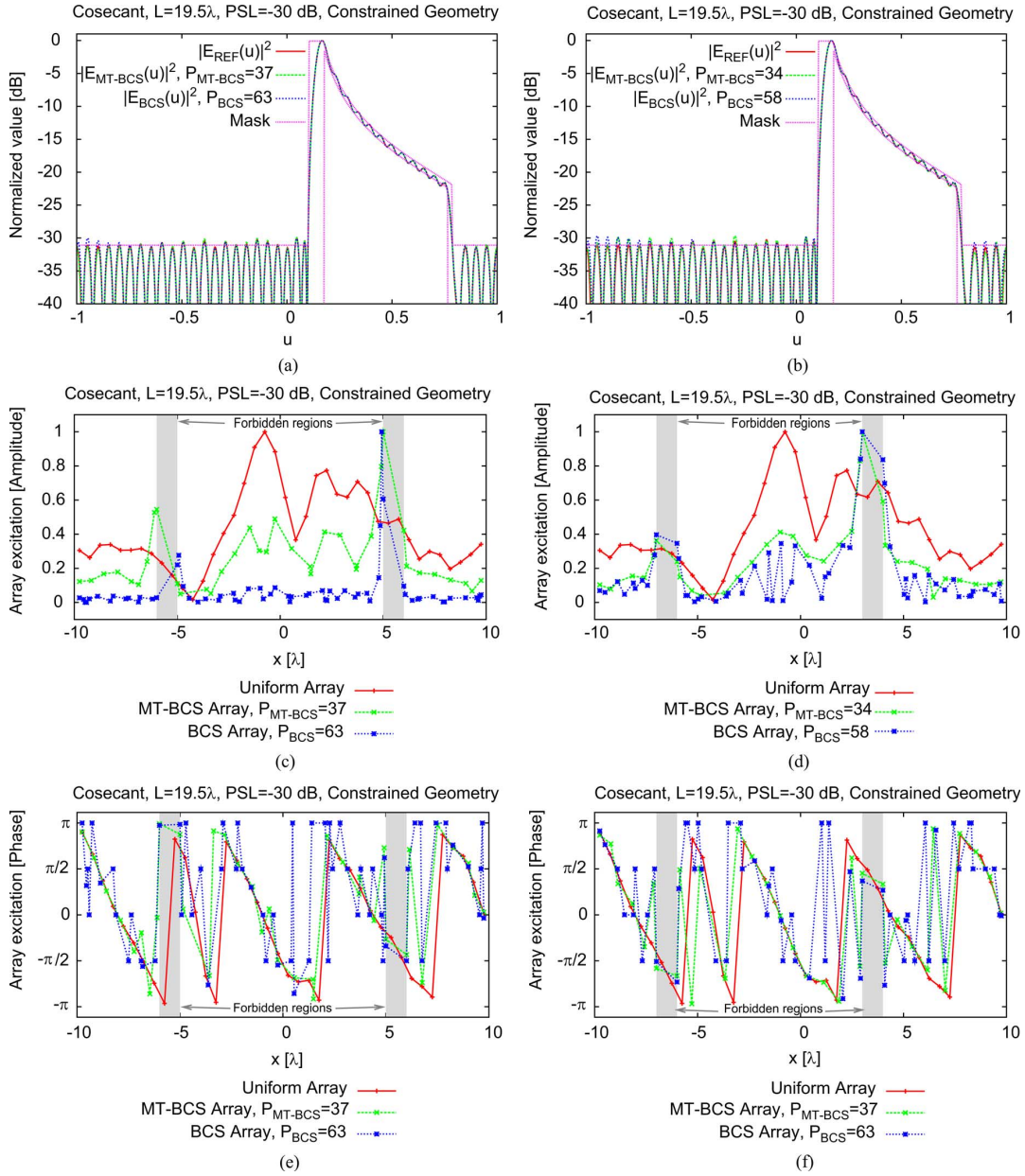


Fig. 15. *Flexibility Check (Constrained-Geometry Pattern Synthesis: “Cosecant,”  $L = 19.5\lambda$ ,  $PSL = -30$  dB,  $P_{REF} = P_{UNI} = 40$ )—Power patterns (a),(b), excitation amplitudes (c),(d), and excitation phases (e),(f) of the (unconstrained) uniform array and of the optimal trade-off constrained BCS and MT–BCS layouts when  $d_n \notin \{[-6\lambda, -5\lambda] \cup [5\lambda, 6\lambda]\}$  (left column) and  $d_n \notin \{[-7\lambda, -6\lambda] \cup [3\lambda, 4\lambda]\}$  (right column).*

Analogously to the *BCS* case,  $\mathcal{P}(\mathbf{w}_H)$  in (17) is used to enforce the “sparseness” of  $\mathbf{w}_H$  (i.e., the minimization of  $\|\mathbf{w}_H\|_{\ell_0}$ ) [18], but besides the *BCS* definition, the *MT–BCS* prior also establishes the interrelationships between  $\mathbf{w}_R$  and  $\mathbf{w}_I$ . Towards this end, a shared prior is placed across the two (i.e.,  $H = R$  and  $H = I$ ) CS “tasks” in (17) [39]. Mathematically, it is assumed that [39]

$$\mathcal{P}(\mathbf{w}_H) = \int \mathcal{P}(\mathbf{w}_H | \hat{\mathbf{a}}, \hat{\sigma}^2) \mathcal{P}(\hat{\mathbf{a}}) \mathcal{P}(\hat{\sigma}^2) d\hat{\mathbf{a}} d\hat{\sigma}^2 \quad (18)$$

where  $\hat{\mathbf{a}} = \{\hat{a}_n; n = 1, \dots, N\}$ ,  $\hat{\mathbf{a}} \in \mathbb{R}^N$ , is the “shared” hyperparameters vector [39], whose associated hyperpriors still comply with the Gamma distribution [39]

$$\mathcal{P}(\hat{\mathbf{a}}) = \prod_{n=1}^N \left[ \frac{\beta_2^{\beta_1} (\hat{a}_n)^{\beta_1-1} e^{-\beta_2 \hat{a}_n}}{\int_0^\infty t^{\beta_1-1} e^{-t} dt} \right] \quad (19)$$

as for the *BCS* [see (5)—[18]]. Moreover, a “shared” Gamma hierarchical prior is enforced on  $\hat{\sigma}^2$  [39] with the same form as in the *BCS* (see (6)—[18])

$$\mathcal{P}(\hat{\sigma}^2) = \frac{\beta_4^{\beta_3} \left( \frac{1}{\hat{\sigma}^2} \right)^{(\beta_3-1)} e^{-\beta_4/\hat{\sigma}^2}}{\int_0^\infty t^{\beta_3-1} e^{-t} dt} \quad (20)$$

where the user-defined coefficients  $\beta_1$ – $\beta_4$  are the so-called “scale priors” [39].

Concerning  $\mathcal{P}(\mathbf{w}_H | \hat{\mathbf{a}}, \hat{\sigma}^2)$ , the following hierarchical Gaussian model is assumed [39]

$$\mathcal{P}(\mathbf{w}_H | \hat{\mathbf{a}}, \hat{\sigma}^2) = \left[ (2\pi\hat{\sigma})^{-N} \right] \prod_{n=1}^N \sqrt{\hat{a}_n} \exp \left[ -\frac{\hat{a}_n (w_n^H)^2}{2\hat{\sigma}^2} \right]. \quad (21)$$

Back substituting (18) in (17), it results that

$$\begin{aligned} \mathbf{w}_H^{MT-BCS} &= \\ &\arg \left\{ \max_{\mathbf{w}_H} \left[ \int \frac{\mathcal{P}(\mathbf{w}_H | \hat{\mathbf{a}}, \hat{\sigma}^2) \mathcal{P}(\hat{\mathbf{F}}_H | \mathbf{w}_H) \mathcal{P}(\hat{\mathbf{a}}) \mathcal{P}(\hat{\sigma}^2)}{\mathcal{P}(\hat{\mathbf{F}}_H)} d\hat{\mathbf{a}} d\hat{\sigma}^2 \right] \right\} \end{aligned} \quad (22)$$

and, by integrating over  $\hat{\sigma}^2$  and performing simple mathematical manipulations, the relation (22) can be rewritten as

$$\begin{aligned} \mathbf{w}_H^{MT-BCS} &= \\ &= \arg \left\{ \max_{\mathbf{w}_H} \left[ \int \mathcal{P}(\mathbf{w}_H | \hat{\mathbf{F}}_H, \hat{\mathbf{a}}) \mathcal{P}(\hat{\mathbf{a}} | \hat{\mathbf{F}}_H) d\hat{\mathbf{a}} \right] \right\}. \end{aligned} \quad (23)$$

As far as the first term in (23) is concerned, one can notice that [39]

$$\mathcal{P}(\mathbf{w}_H | \hat{\mathbf{F}}_H, \hat{\mathbf{a}}) = \int \mathcal{P}(\mathbf{w}_H | \hat{\mathbf{F}}_H, \hat{\mathbf{a}}, \hat{\sigma}^2) \mathcal{P}(\hat{\sigma}^2) d\hat{\sigma}^2 \quad (24)$$

whose integrand is given by

$$\begin{aligned} &\mathcal{P}(\mathbf{w}_H | \hat{\mathbf{F}}_H, \hat{\mathbf{a}}, \hat{\sigma}^2) \mathcal{P}(\hat{\sigma}^2) \\ &= \frac{\mathcal{P}(\hat{\mathbf{F}}_H | \mathbf{w}_H, \hat{\sigma}^2) \mathcal{P}(\mathbf{w}_H | \hat{\mathbf{a}}, \hat{\sigma}^2) \mathcal{P}(\hat{\sigma}^2)}{\int \mathcal{P}(\hat{\mathbf{F}}_H | \mathbf{w}_H, \hat{\sigma}^2) \mathcal{P}(\mathbf{w}_H | \hat{\mathbf{a}}, \hat{\sigma}^2) d\mathbf{w}_H} \end{aligned} \quad (25)$$

according to Bayes' theorem. By using (20) and (21), and observing that [see (11)]

$$\begin{aligned} &\mathcal{P}(\hat{\mathbf{F}}_H | \mathbf{w}_H, \hat{\sigma}^2) \\ &= \frac{1}{(2\pi\hat{\sigma}^2)^{K/2}} \exp \left( -\frac{1}{2\hat{\sigma}^2} \|\hat{\mathbf{F}}_H - \hat{\Phi}\mathbf{w}_H\|^2 \right), \end{aligned} \quad (26)$$

it results that

$$\begin{aligned} \mathcal{P}(\mathbf{w}_H | \hat{\mathbf{F}}_H, \hat{\mathbf{a}}) &= \left( \int_0^\infty t^{\beta_1+N/2-1} e^{-t} dt \right) \\ &\times \frac{\left[ 1 + \frac{1}{2\beta_2} (\mathbf{w}_H - \hat{\mu}_H)^T \hat{\Sigma}^{-1} (\mathbf{w}_H - \hat{\mu}_H) \right]^{-(\beta_1+N/2)}}{\left( \int_0^\infty t^{\beta_1-1} e^{-t} dt \right) (2\pi\beta_2)^{N/2} \sqrt{|\hat{\Sigma}|}} \end{aligned} \quad (27)$$

where  $\hat{\mu}_H \triangleq \hat{\Sigma}\hat{\Phi}^T\hat{\mathbf{F}}_H$  and  $\hat{\Sigma} \triangleq (\hat{A} + \hat{\Phi}^T\hat{\Phi})^{-1}$ , being  $\hat{A} \triangleq \text{diag}(\hat{\mathbf{a}})$ . By analyzing the expression of  $\mathcal{P}(\mathbf{w}_H | \hat{\mathbf{F}}_H, \hat{\mathbf{a}})$ , it is worth noticing that the posterior distribution over  $\mathbf{w}_H$  is now a multivariate *Student-t* distribution (27) instead of the multi-variate Gaussian distribution of the *BCS* ((9)–[18]). Moreover, the scale terms  $\beta_3$  and  $\beta_4$  do not have to be specified unlike  $\beta_1$  and  $\beta_2$  since the corresponding distributions are not explicitly required for the computations. Concerning the remaining term in the integral of (23), a “delta-function” approximation is adopted analogously to the *BCS* case [39] since its closed-form

computation is not feasible. Towards this end, let us firstly notice that

$$\mathcal{P}(\hat{\mathbf{a}} | \hat{\mathbf{F}}_H) \propto \mathcal{P}(\hat{\mathbf{F}}_H | \hat{\mathbf{a}}) \mathcal{P}(\hat{\mathbf{a}})$$

or in a different fashion

$$\begin{aligned} \mathcal{P}(\hat{\mathbf{a}} | \hat{\mathbf{F}}_H) &\propto \left[ \int \mathcal{P}(\hat{\mathbf{F}}_H | \mathbf{w}_H, \hat{\sigma}^2) \mathcal{P}(\mathbf{w}_H | \hat{\mathbf{a}}, \hat{\sigma}^2) \right. \\ &\quad \left. \times \mathcal{P}(\hat{\sigma}^2) d\mathbf{w}_H d\hat{\sigma}^2 \right] \mathcal{P}(\hat{\mathbf{a}}) \end{aligned} \quad (28)$$

whose *mode* (over the two tasks  $H \in \{R, I\}$ ) can be computed, by using (26), (20), and (21), as [39]

$$\hat{\mathbf{a}}^{MT-BCS} = \arg \max_{\hat{\mathbf{a}}} \{ \mathcal{L}^{MT-BCS}(\hat{\mathbf{a}}) \} \quad (29)$$

where  $\mathcal{L}^{MT-BCS}(\hat{\mathbf{a}})$  is the logarithm of the *MT-BCS* “marginal likelihood” given by

$$\begin{aligned} \mathcal{L}^{MT-BCS}(\hat{\mathbf{a}}) &= -\frac{1}{2} \sum_H \left\{ \log \left( \left| I + \hat{\Phi} [\hat{A}]^{-1} \hat{\Phi}^T \right| \right) + \right. \\ &\quad \left. + (N+2\beta_1) \log \left[ \hat{\mathbf{F}}_H^T \left( I + \hat{\Phi} [\hat{A}]^{-1} \hat{\Phi}^T \right) \hat{\mathbf{F}}_H + 2\beta_2 \right] \right\}. \end{aligned} \quad (30)$$

By using (29), the *delta-function* approximation is then applied to obtain

$$\mathcal{P}(\hat{\mathbf{a}} | \hat{\mathbf{F}}_H) \approx \delta(\hat{\mathbf{a}} - \hat{\mathbf{a}}^{MT-BCS}). \quad (31)$$

By substituting (27) and (31) in (23) and since the mode of a multi-variate *Student-t* distribution is equal to its average value (i.e.,  $\hat{\mu}_H$ ), it turns out that

$$\begin{aligned} &\mathbf{w}_H|_{MTBCS} \\ &= \arg \left\{ \max_{\mathbf{w}_H} \left[ \int \mathcal{P}(\mathbf{w}_H | \hat{\mathbf{F}}_H, \hat{\mathbf{a}}) \delta(\hat{\mathbf{a}} - \hat{\mathbf{a}}^{MT-BCS}) d\hat{\mathbf{a}} \right] \right\} \\ &= \arg \left\{ \max_{\mathbf{w}_H} \left[ \mathcal{P}(\mathbf{w}_H | \hat{\mathbf{F}}_H, \hat{\mathbf{a}}) \right]_{\hat{\mathbf{a}}=\hat{\mathbf{a}}^{MT-BCS}} \right\} \\ &= \hat{\mu}_H|_{\hat{\mathbf{a}}=\hat{\mathbf{a}}^{MT-BCS}}. \end{aligned} \quad (32)$$

## ACKNOWLEDGMENT

The authors wish to thank Prof. A. Trucco for kindly providing some numerical results for the test cases in [17] and Dr. S. Ji, Dr. Y. Xue, and Prof. L. Carin for sharing the *BCS* and *MT-BCS* code online [50].

## REFERENCES

- [1] R. J. Mailloux, *Phased Array Antenna Handbook*, 2nd ed. Norwood, MA: Artech House, 2005.
- [2] R. S. Elliot and J. G. Stern, “Optimizing synthesis of shaped beam antenna patterns,” *IEEE Trans. Antennas Propag.*, vol. 32, no. 10, pp. 1129–1133, Oct. 1984.
- [3] T. Isernia, O. M. Bucci, and N. Fiorentino, “Shaped beam antenna synthesis problems: Feasibility criteria and new strategies,” *J. Electromagn. Waves Appl.*, vol. 12, pp. 103–137, 1998.
- [4] T. Isernia and G. Panariello, “Optimal focusing of scalar fields subject to arbitrary upper bounds,” *Electron. Lett.*, vol. 34, no. 2, pp. 162–164, Jan. 1998.

- [5] O. M. Bucci, L. Caccavale, and T. Isernia, "Optimal far-field focusing of uniformly spaced arrays subject to arbitrary upper bounds in non-target directions," *IEEE Trans. Antennas Propag.*, vol. 50, no. 11, pp. 1539–1554, Nov. 2002.
- [6] R. M. Leahy and B. D. Jeffs, "On the design of maximally sparse beam-forming arrays," *IEEE Trans. Antennas Propag.*, vol. 39, no. 8, pp. 1178–1187, Aug. 1991.
- [7] R. F. Harrington, "Sidelobe reduction by nonuniform element spacing," *IEEE Trans. Antennas Propag.*, vol. 9, p. 187, Mar. 1961.
- [8] M. G. Andreasan, "Linear arrays with variable interelement spacings," *IEEE Trans. Antennas Propag.*, vol. 10, pp. 137–143, Mar. 1962.
- [9] A. Ishimaru, "Theory of unequally-spaced arrays," *IEEE Trans. Antennas Propag.*, vol. 11, pp. 691–702, Nov. 1962.
- [10] D. G. Leeper, "Isophoric arrays—massively thinned phased arrays with well-controlled sidelobes," *IEEE Trans. Antennas Propag.*, vol. 47, no. 12, pp. 1825–1835, Dec. 1999.
- [11] Y. Liu, Z. Nie, and Q. H. Liu, "Reducing the number of antenna elements in a linear antenna array by the matrix pencil method," *IEEE Trans. Antennas Propag.*, vol. 56, no. 9, pp. 2955–2962, Sep. 2008.
- [12] D. King, R. Packard, and R. Thomas, "Unequally spaced, broad-band antenna arrays," *IRE Trans. Antennas Propag.*, vol. 8, pp. 380–384, Jul. 1960.
- [13] A. Maffett, "Array factors with nonuniform spacing arrays," *IRE Trans. Antennas Propag.*, vol. 10, pp. 131–136, Mar. 1962.
- [14] N. Balakrishnan, P. Murthy, and S. Ramakrishna, "Synthesis of antenna arrays with spatial and excitation constraints," *IEEE Trans. Antennas Propag.*, vol. 29, pp. 690–696, Sep. 1962.
- [15] G. Oliveri, M. Donelli, and A. Massa, "Linear array thinning exploiting almost difference sets," *IEEE Trans. Antennas Propag.*, vol. 57, no. 12, pp. 3800–3812, Dec. 2009.
- [16] V. Murino, A. Trucco, and C. S. Regazzoni, "Synthesis of unequally spaced arrays by simulated annealing," *IEEE Trans. Signal Processing*, vol. 44, no. 1, pp. 119–123, Jan. 1996.
- [17] A. Trucco and V. Murino, "Stochastic optimization of linear sparse arrays," *IEEE J. Oceanic Engineering*, vol. 24, no. 3, pp. 291–299, Jul. 1999.
- [18] G. Oliveri and A. Massa, "Bayesian compressive sampling for pattern synthesis with maximally sparse non-uniform linear arrays," *IEEE Trans. Antennas Propag.*, vol. 59, no. 2, pp. 467–481, Feb. 2011.
- [19] Y. T. Lo, "A mathematical theory of antenna arrays with randomly spaced elements," *IEEE Trans. Antennas Propag.*, vol. 12, no. 3, pp. 257–268, May 1964.
- [20] B. Steinberg, "The peak sidelobe of the phased array having randomly located elements," *IEEE Trans. Antennas Propag.*, vol. 20, no. 2, pp. 129–136, Mar. 1972.
- [21] M. I. Skolnik, G. Nemhauser, and J. W. Sherman, "Dynamic programming applied to unequally-space arrays," *IRE Trans. Antennas Propag.*, vol. AP-12, pp. 35–43, Jan. 1964.
- [22] R. L. Haupt, "Thinned arrays using genetic algorithms," *IEEE Trans. Antennas Propag.*, vol. 42, no. 7, pp. 993–999, Jul. 1994.
- [23] T. G. Spence and D. H. Werner, "Thinning of aperiodic antenna arrays for low side-lobe levels and broadband operation using genetic algorithms," in *Proc. IEEE Antennas and Propagation Society Int. Symp.*, Jul. 9–14, 2006, pp. 2059–2062.
- [24] R. L. Haupt and D. H. Werner, *Genetic Algorithms in Electromagnetics*. Hoboken, NJ: Wiley, 2007.
- [25] G. Oliveri, L. Manica, and A. Massa, "ADS-based guidelines for thinned planar arrays," *IEEE Trans. Antennas Propag.*, vol. 58, no. 6, pp. 1935–1948, Jun. 2010.
- [26] S. Caorsi, A. Lommi, A. Massa, and M. Pastorino, "Peak sidelobe reduction with a hybrid approach based on GAs and difference sets," *IEEE Trans. Antennas Propag.*, vol. 52, no. 4, pp. 1116–1121, Apr. 2004.
- [27] P. J. Bevelacqua and C. A. Balanis, "Minimum sidelobe levels for linear arrays," *IEEE Trans. Antennas Propag.*, vol. 55, pp. 2210–2217, Dec. 2007.
- [28] M. Donelli, A. Martini, and A. Massa, "A hybrid approach based on PSO and Hadamard difference sets for the synthesis of square thinned arrays," *IEEE Trans. Antennas Propag.*, vol. 57, no. 8, pp. 2491–2495, Aug. 2009.
- [29] G. Oliveri and A. Massa, "Genetic algorithm (GA)-enhanced almost difference set (ADS)-based approach for array thinning," *IET Microw. Antennas Propag.*, vol. 5, no. 3, pp. 305–315, Feb. 2011.
- [30] Y. Liu, Z. Nie, and Q. H. Liu, "A new method for the synthesis of non-uniform linear arrays with shaped power patterns," *Prog. Electromagn. Res.*, vol. 107, pp. 349–363, 2010.
- [31] Y. Liu, Q. H. Liu, and Z. Nie, "Reducing the number of elements in the synthesis of shaped-beam pattern by the forward-backward matrix pencil method," *IEEE Trans. Antennas Propag.*, vol. 58, no. 2, pp. 604–608, Feb. 2010.
- [32] J. Perini and M. Idselis, "Note on antenna pattern synthesis using numerical iterative methods," *IEEE Trans. Antennas Propag.*, vol. 19, no. 2, pp. 284–286, Mar. 1971.
- [33] R. W. Redlich, "Iterative least-squares of nonuniformly spaced linear arrays," *IEEE Trans. Antennas Propag.*, vol. 21, no. 1, pp. 106–108, Jan. 1973.
- [34] S. Holm, B. Elgetun, and G. Dahl, "Properties of the beampattern of weight- and layout-optimized sparse arrays," *IEEE Trans. Ultrason., Ferroelectr., Freq. Control*, vol. 44, no. 5, pp. 983–991, Sep. 1997.
- [35] B. P. Kumar and G. R. Branner, "Design of unequally spaced arrays for performance improvement," *IEEE Trans. Antennas Propag.*, vol. 47, pp. 511–523, Mar. 1999.
- [36] B. P. Kumar and G. R. Branner, "Generalized analytical technique for the synthesis of unequally spaced arrays with linear, planar, cylindrical or spherical geometry," *IEEE Trans. Antennas Propag.*, vol. 53, pp. 621–633, Feb. 2005.
- [37] F. B. T. Marchaud, G. D. de Villiers, and E. R. Pike, "Element positioning for linear arrays using generalized Gaussian quadrature," *IEEE Trans. Antennas Propag.*, vol. 51, no. 6, pp. 1357–1363, Jun. 2003.
- [38] S. Ji, Y. Xue, and L. Carin, "Bayesian compressive sensing," *IEEE Trans. Signal Process.*, vol. 56, no. 6, pp. 2346–2356, Jun. 2008.
- [39] S. Ji, D. Dunson, and L. Carin, "Multi-task compressive sampling," *IEEE Trans. Signal Process.*, vol. 57, no. 1, pp. 92–106, Jan. 2009.
- [40] M. E. Tipping and A. C. Faul, C. M. Bishop and B. J. Frey, Eds., "Fast marginal likelihood maximization for sparse Bayesian models," in *Proc. 9th Int. Workshop Artificial Intelligence and Statistics*, 2003 [Online]. Available: <http://citeseer.ist.psu.edu/611465.html>
- [41] A. C. Faul and M. E. Tipping, T. G. Dietterich, S. Becker, and Z. Ghahramani, Eds., "Analysis of sparse Bayesian learning," in *Advances in Neural Information Processing Systems (NIPS 14)*, 2002, pp. 383–389 [Online]. Available: <http://citeseer.ist.psu.edu/faul01analysis.html>
- [42] M. E. Tipping, "Sparse bayesian learning and the relevance vector machine," *J. Machine Learning Res.*, vol. 1, pp. 211–244, 2001.
- [43] A. Akdagli and K. Guney, "Shaped-beam pattern synthesis of equally and unequally spaced linear antenna arrays using a modified tabu search algorithm," *Microwave Opt. Technol. Lett.*, vol. 36, no. 1, pp. 16–20, 2003.
- [44] S. Yang, Y. Liu, and Q. H. Liu, "Combined strategies based on matrix pencil method and tabu search algorithm to minimize elements of non-uniform antenna array," *Prog. Electromagn. Res. B*, vol. 18, pp. 259–277, 2009.
- [45] D. Marciano and F. Duran, "Synthesis of antenna arrays using genetic algorithms," *IEEE Antennas Propag. Mag.*, vol. 42, no. 3, pp. 12–22, Jun. 2000.
- [46] A. Akdagli and K. Guney, "Touring ant colony optimization algorithm for shaped beam pattern synthesis of linear antenna arrays," *Electromagnetics*, vol. 25, no. 6, pp. 615–628, Aug. 2006.
- [47] J. M. Cid, J. A. Rodriguez, and F. Ares, "Shaped power patterns produced by equispaced linear arrays: Optimized synthesis using orthogonal  $\sin(Nx)/\sin(x)$  beams," *J. Electromagn. Waves Appl.*, vol. 13, no. 7, pp. 985–992, 1999.
- [48] S. A. Vorobyov, A. B. Gershman, and K. W. Wong, "Maximum likelihood direction-of-arrival estimation in unknown noise fields using sparse sensor arrays," *IEEE Trans. Signal Process.*, vol. 53, no. 1, pp. 34–43, Jan. 2005.
- [49] L. Lei, J. P. Lie, A. B. Gershman, and C. M. S. See, "Robust adaptive beamforming in partly calibrated sensor arrays," *IEEE Trans. Signal Process.*, vol. 58, no. 3, pp. 1661–1667, Mar. 2005.
- [50] S. Ji, Y. Xue, and L. Carin, "Single-Task and Multi-Task Bayesian Compressive Sensing Code," 2009.



**Giacomo Oliveri** (M'09) received the B.S. (*summa cum laude*) and M.S. (*summa cum laude*) degrees in telecommunications engineering and the Ph.D. degree in space sciences and engineering from the University of Genoa, Italy, in 2003, 2005, and 2009 respectively.

He is currently a member of the ELEDIA Research Center at the University of Trento, Italy. He is author/coauthor of over 100 peer reviewed papers on international journals and conferences. His research work is mainly focused on cognitive radio systems,

electromagnetic direct and inverse problems, and antenna array design and synthesis.



**Matteo Carlin** received the first level degree and the “Laurea Specialistica” (M.S.) degree in telecommunication engineering from the University of Trento, Italy, in 2008 and 2010, respectively. He is currently working toward the Ph.D. degree at the ICT International Doctoral School of Trento.

He is a member of the ELEDIA Research Center at the University of Trento, Italy. His research interests are in the area of electromagnetic inverse scattering and antenna array design and synthesis.



**Andrea Massa** (M’96) received the “Laurea” degree in electronic engineering and Ph.D. degree in electronics and computer science from the University of Genoa, Genoa, Italy, in 1992 and 1996, respectively.

From 1997 to 1999, he was an Assistant Professor of electromagnetic fields at the Department of Bio-physical and Electronic Engineering (University of Genoa) teaching the university course of Electromagnetic Fields 1. From 2001 to 2004, he was an Associate Professor at the University of Trento. Since 2005, he has been a Full Professor of electromag-

netic fields at the University of Trento, where he currently teaches electromagnetic fields, inverse scattering techniques, antennas and wireless communications, and optimization techniques. At present, he is the Director of the ELEDIA Research Center at the University of Trento and Deputy Dean of the Faculty of Engineering. Moreover, he is Adjunct Professor at Penn State University (USA), and Visiting Professor at the Missouri University of Science and Technology (USA), at the Nagasaki University (Japan) and at the University of Paris Sud (France). His research work since 1992 has been principally focused on electromagnetic direct and inverse scattering, microwave imaging, optimization techniques, wave propagation in presence of nonlinear media, wireless communications and applications of electromagnetic fields to telecommunications, medicine and biology.

Prof. Massa is a member of the IEEE Society, the PIERS Technical Committee, and the Inter-University Research Center for Interactions Between Electromagnetic Fields and Biological Systems (ICEmB). He is the Italian representative in the general assembly of the European Microwave Association (EuMA). He serves as an Associate Editor of the IEEE TRANSACTIONS ON ANTENNAS AND PROPAGATION.